term on the right hand side is taken into account, this relation is called Weyl's law. The last two terms have the following meaning:

$$b(\gamma_i) = \frac{1}{2\pi}\int_{\gamma_i} K(l)\mathrm{d}l \ , \tag{140}$$

which is an integral over the curvature $K(l)$ along the boundary curve γ_i, and

$$c(\alpha_j) = \frac{1}{24}\left(\frac{\pi}{\alpha_j} - \frac{\alpha_j}{\pi}\right) \ , \ 0 < \alpha_j \leq 2\pi. \tag{141}$$

For many systems formula (139) is a very good approximation to the function $\bar{N}(E)$ down to the lowest energy eigenvalue, so that the asymptotic formula can also be applied in the low-energy regime.

Clearly, formula (139) cannot be applied to the hyperbola billiard, which has an infinite area. But Weyl's law can be used in an intuitive argument for the determination of the leading asymptotic behaviour of $\bar{N}(E)$ [50]. A solution of the Schrödinger equation of the hyperbola billiard with energy E typically has a significant value for the amplitude only in those parts of the billiard region, where the distance of the two opposite boundary curves in the horns is not smaller than the de Broglie wavelength. This leads to the definition of an effective area for this wavefunction, which is given by

$$A_{eff} = 1 + 2\log(1/\lambda_E) = 1 + 2\log(\sqrt{E}/2\pi) \ , \tag{142}$$

where $\lambda_E = 2\pi/\sqrt{E}$ is the de Broglie wavelength in dimensionless units. With eq. (142) the leading asymptotic term for $\bar{N}(E)$ follows as

$$\bar{N}(E) \sim \frac{1}{4\pi} E\log E \ , \ E \to \infty \ . \tag{143}$$

It was shown by Simon [86] that this is indeed the correct asymptotic behaviour. The next leading terms in the asymptotic formula for $\bar{N}(E)$ were derived by Steiner and Trillenberg [87]. Separated into contributions from even and odd wavefunctions the result is

$$\bar{N}^{\pm}(E) = \frac{1}{8\pi}E\log E + \frac{a}{8\pi}E + \frac{1}{8\pi}b^{\pm}\sqrt{E} + O(E^{1/4}\log E) \ , \ E \to \infty \tag{144}$$

$$a = 2(\gamma - \log 2\pi) \ , \ b^{\pm} = 4\frac{\pi^{3/2}}{\Gamma^2(1/4)} \pm 2\sqrt{2} \ .$$

In figure 11 a) the two functions $\bar{N}^{+}(E)$ and $\bar{N}^{-}(E)$ are compared to the numerically calculated staircase functions $N^{+}(E)$ and $N^{-}(E)$, respectively. The agreement is excellent over the whole energy range, so that for both symmetry subspaces of the energy spectrum the curves for $N(E)$ and $\bar{N}(E)$ cannot be resolved within the given scale. For that reason figure 11 b) shows a section of figure 11 a) for the energy range $1400 < E < 1500$.

The correction terms for eq. (144) are not known analytically, but they can be determined numerically. For that reason the deviation of the spectral staircase $N(E)$ from $\bar{N}(E)$ is examined in both symmetry subspaces. Mean energies $\bar{E}_n$ which are defined by means of the the generalized Weyl's law eq. (144) are given by

$$\bar{N}(\bar{E}_n) = n - 1/2 \ . \tag{145}$$

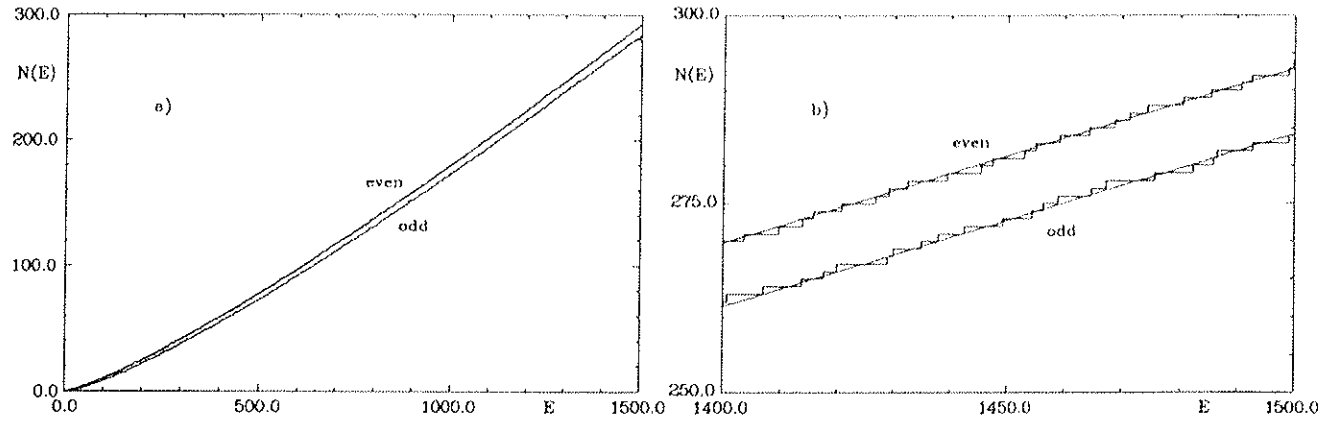

Figure 11: The spectral staircase $N(E)$ in comparison with the generalized Weyl's law eq. (144) for even and odd energy eigenfunctions within the energy ranges a) $0 < E < 1500$ and b) $1400 < E < 1500$.

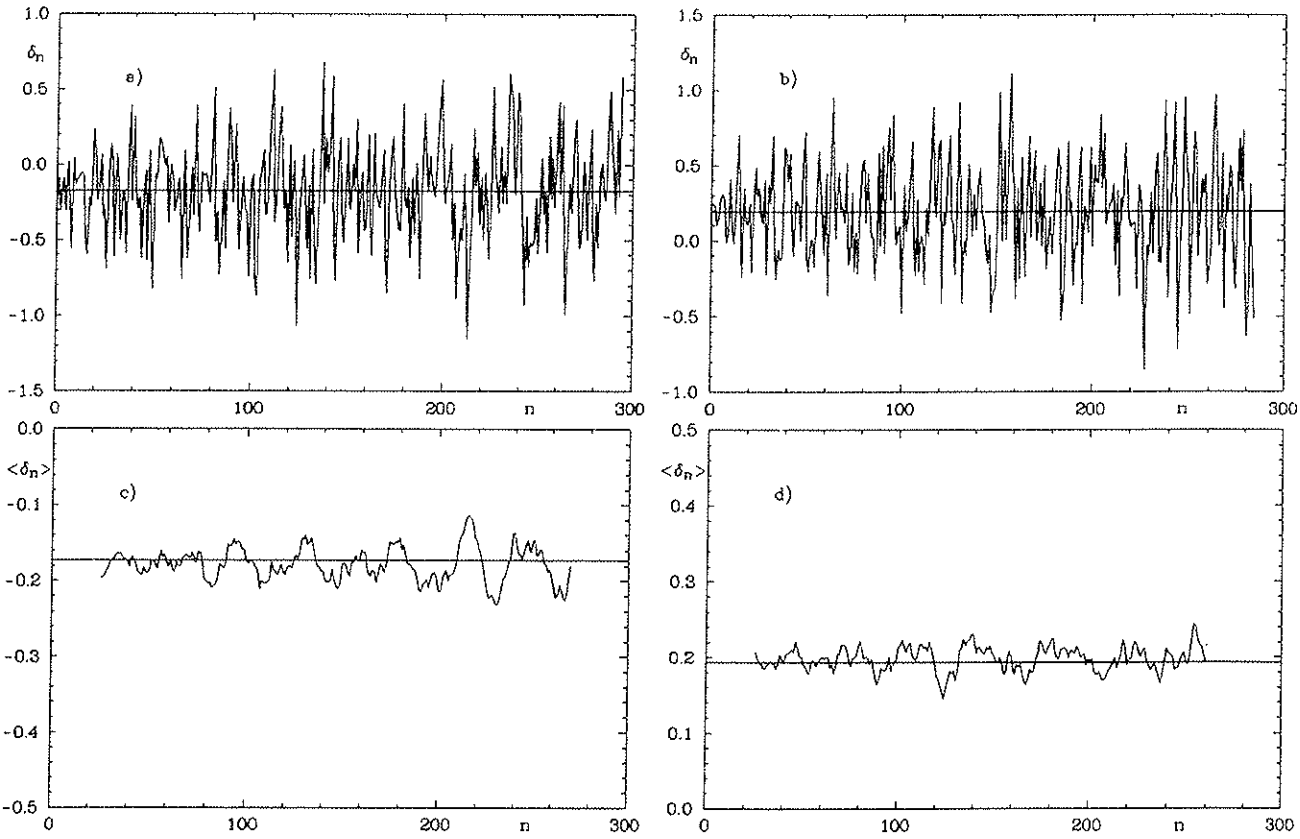

Figure 12: The deviations δ_n from the generalized Weyl's law eq. (144) for the energies of a) even and b) odd wave functions. c) and d) show the results of smoothing the curves in a) and b), respectively, over a range of 50 energies. The horizontal lines represent the mean values of the deviations δ_n.

For that reason the quantities

$$\delta_n = n \quad 1/2 \quad N(E_n) \tag{146}$$

are a measure of the deviation of the numerically obtained spectrum from $\bar{N}(E)$.

In figure 12 a) and b) the quantities δ_n are shown for even and odd symmetries. The horizontal lines represent the mean values of the δ_n. Figures 12 c) and d) show the same curves smoothed over a range of 50 energies. As can be seen the approximation to the functions $\bar{N}^+(E)$ and $\bar{N}^-(E)$, which is given by eq. (144), is equally good in the lower and higher energy range. Within the numerical accuracy the next correction term to eq. (144) is in both cases a constant with value $c^+ = -0.173$ and $c^- = 0.194$, respectively.

For an interpretation of this result it is assumed in the following that the contributions of the corners and of the curvature of the boundary to $\bar{N}(E)$ is the same as for bounded billiards. For example, the contribution of the part of the boundary along the line $y = x$, which leads to the difference between $\bar{N}^+(E)$ and $\bar{N}^-(E)$, is also the same as for finite billiards. On this assumption the constant contributions to $\bar{N}^+(E)$ and $\bar{N}^-(E)$ are given by

$$c^+ = -c\left(\frac{\pi}{4}\right) + b(C) + c_{horn} = -\frac{9}{32} + c_{horn} \tag{147}$$

and

$$c^- = c\left(\frac{\pi}{2}\right) + c\left(\frac{\pi}{4}\right) + b(C) + c_{horn} = \frac{3}{32} + c_{horn} \ , \tag{148}$$

respectively. $C = \{(x, 1/x) | 1 \leq x < \infty\}$ denotes the curved part of the boundary. The constant contributions to $\bar{N}^+(E)$ for even wavefunctions, which satisfy partly Dirichlet and partly Neumann boundary conditions on the boundary of the desymmetrized billiard system, are obtained by the difference between the constant contributions to $\bar{N}(E)$ for the full system and the constant contributions to $\bar{N}^-(E)$. The curvature term is calculated as

$$b(C) = -\frac{1}{2\pi}\int_1^\infty \frac{2x^3}{(1+x^4)^{3/2}}\frac{\sqrt{x^4+1}}{x^2}\,\mathrm{d}x = -\frac{1}{\pi}\int_1^\infty \frac{x}{1+x^4}\,\mathrm{d}x = -\frac{1}{8} \ . \tag{149}$$

c_{horn} denotes possible contributions to c^+ and c^- from the infinite horn. The difference between both constants is $\Delta c := c^+ - c^- = -0.375$, which is in very good agreement with the numerically obtained value $\Delta c = -0.367$. From this one obtains a value of

$$c_{horn} = 0.10 \tag{150}$$

for the constant c_{horn}.

IV.3 The Level Spacings Distribution

The most frequently used energy statistics is the distribution $P(S)$ of spacings between neighbouring levels. The behaviour of $P(S)$ for small spacings S is significantly different for systems which are classically chaotic and those which are classically integrable. In the integrable case one typically has level clustering, which is expressed by $P(S) \to 1$ as $S \to 0$, while chaotic systems show level repulsion, which implies $P(S) \to 0$ as $S \to 0$.

$P(S)$ is calculated for the scaled energy spectrum, which has a mean level spacing of one. This is obtained with the use of the generalized Weyl's law eq. (144).

$$E'_n = \bar{N}(E_n) \ . \tag{151}$$

Quantities concerning the scaled spectrum are denoted by a prime in the following. For example the spectral staircase for the scaled energies is given by

$$N'(E') = N(E(E')) \quad . \tag{152}$$

The functional form of $P(S)$ which is expected for classically integrable systems is that of a Poisson distribution

$$P(S) = e^{-S} \quad . \tag{153}$$

The result of random-matrix theory for the level spacings distribution of the GOE-ensemble is approximated well by the Wigner distribution

$$P(S) = \frac{\pi}{2} S \exp\left\{-\frac{\pi}{4} S^2\right\} \quad . \tag{154}$$

The corresponding approximation for the distribution $P(S)$ of the GUE-ensemble is given by

$$P(S) = \frac{32}{\pi^2} S^2 \exp\left\{-\frac{4}{\pi} S^2\right\} \quad . \tag{155}$$

The hyperbola billiard has a classically chaotic dynamics with time-reversal symmetry. For that reason it is expected that the statistics of level spacings is that of the GOE-ensemble, provided that it is evaluated separately for the energies of even and odd wavefunctions.

In figure 13 level spacings distributions are shown for the energy range $300 < E < 1500$. In figure 13 a) and b) P(S) is plotted for even and odd wavefunctions, respectively. Both distributions agree with the GOE-expectation. In the odd case the agreement with the GOE-curve is slightly better than in the even case. There are less very long and very short spacings than expected, but the deviations are not statistically significant. In figure 13 c) the distribution of all even-even and odd-odd spacings is plotted in order to improve the statistics. Figure 13 d) shows the distribution $P(S)$ of the total spectrum without separating with respect to symmetry classes. It is compared to a superposition of two independent GOE sequences. Again there are slightly less very short and very long spacings than expected.

The most significant feature of the hyperbola billiard are its horns. As the energy is increased, the wavefunctions explore more and more space in the horns, which is expressed by an increase of the effective area defined in eq. (142). On the other hand the local divergence of neighbouring classical trajectories becomes smaller and smaller as one moves into one of the horns. This is also expressed by the fact that the Lyapunov exponents of non-periodic trajectories decrease on an average as their lengths is increased, since they explore more and more space in the horns.

It is of interest to see, if this classical behaviour has any correspondence in the quantum mechanical energy statistics. In figure 14 a) and b) the statistics of spacings is shown for the energy ranges $300 < E < 900$ and $900 < E < 1500$, respectively. Because of the smaller number of spacings in the considered energy ranges, only the distributions of all spacings within both symmetry subspaces are plotted. In figure 14 there is no significant chance observed in the distribution $P(S)$.

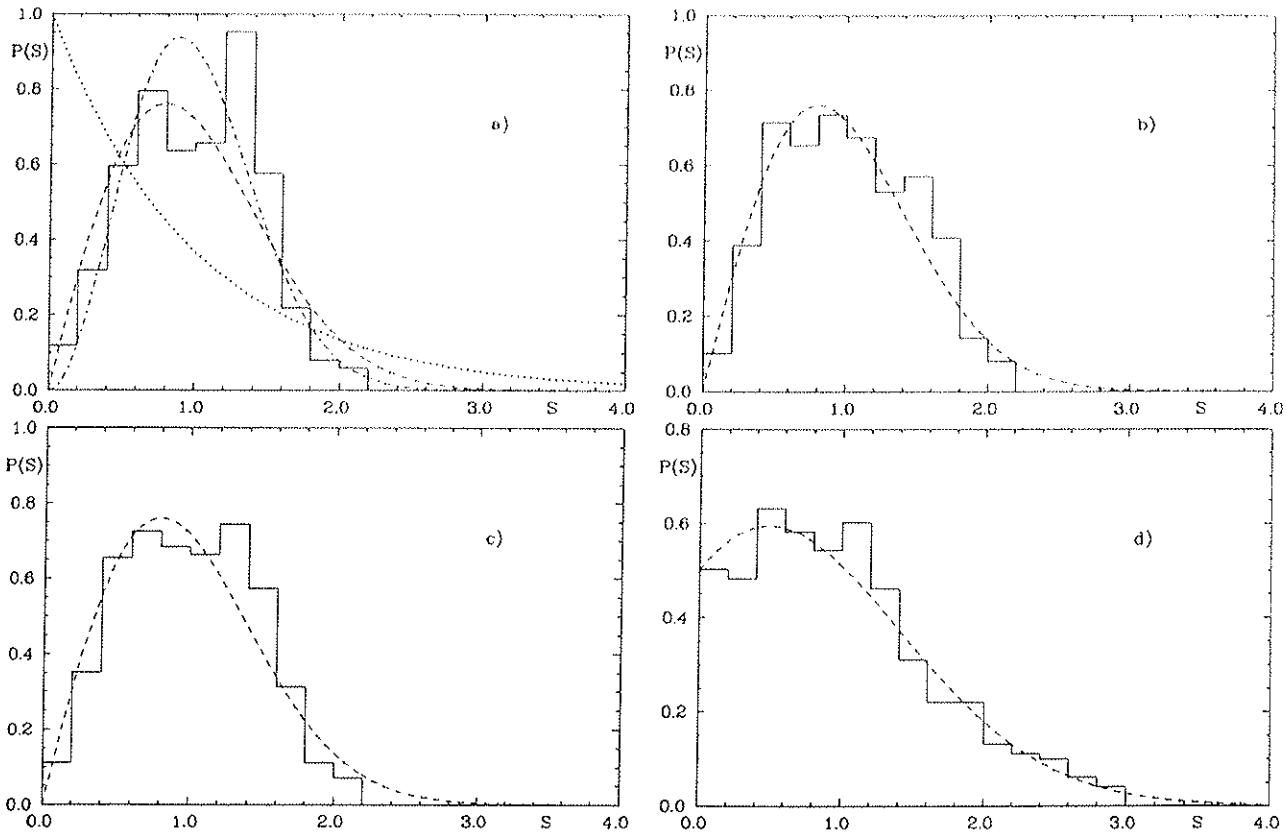

Figure 13: The level spacings distribution for a) even wave functions, b) odd wave functions, c) even and odd wave functions, d) the total energy spectrum. Dotted line: Poisson distribution, dashed-dotted line: GUE expectation, dashed line: in a)-c) GOE expectation, in d) expectation for the superposition of two independent GOE sequences. Energy range: $300 < E < 1500$.

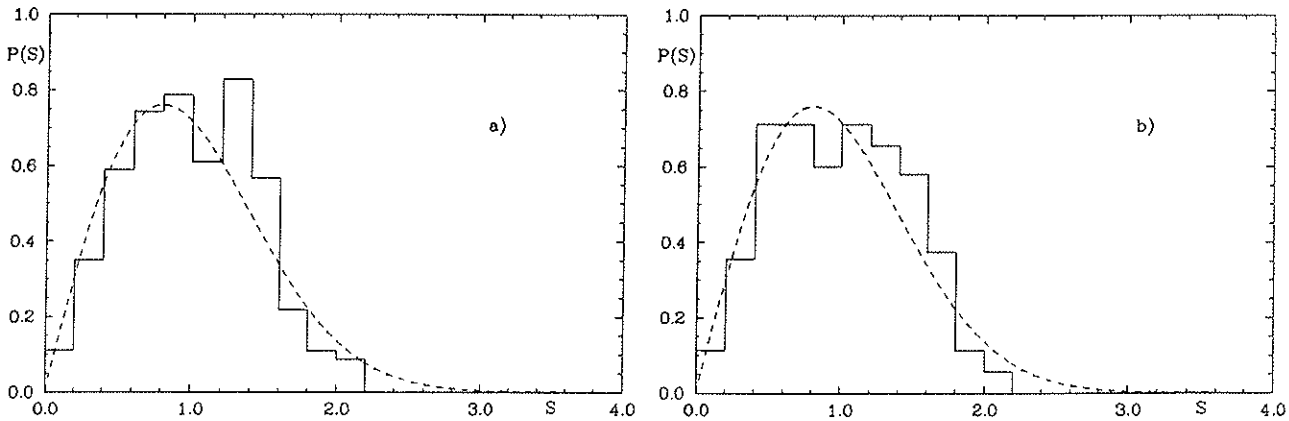

Figure 14: The level spacings distribution for all even-even and odd-odd spacings within the energy ranges a) $300 < E < 900$ and b) $900 < E < 1500$.

IV.4 The Spectral Rigidity and the Number Variance

The spacings distribution $P(S)$ is a short-range statistics. Statistical functions which give information about short-range as well as long-range correlations are the number variance $\Sigma^2(L)$ and the spectral rigidity $\Delta_3(L)$, which are defined in equations (123) and (124), respectively. In terms of the scaled energy spectrum the number variance is defined as the local variance of the number $n(E', L)$ of scaled energy levels in the energy interval from $E' - L/2$ to $E' + L/2$:

$$\Sigma^2(L) = \left\langle [n(E', L) - L]^2 \right\rangle \quad , \tag{156}$$

and the rigidity $\Delta_3(L)$ is given by

$$\begin{aligned} \Delta_3(L) &= \left\langle \frac{1}{L} \int_{-L/2}^{L/2} \mathrm{d}\varepsilon \, N'^2(E' + \varepsilon) - \left[\frac{1}{L} \int_{-L/2}^{L/2} \mathrm{d}\varepsilon \, N'(E' + \varepsilon) \right]^2 \right. \\ &\quad \left. - 12 \left[\frac{1}{L^2} \int_{-L/2}^{L/2} \mathrm{d}\varepsilon \, \varepsilon N'(E' + \varepsilon) \right]^2 \right\rangle \quad . \end{aligned} \tag{157}$$

The relation between both statistics is expressed by eq. (126).

Poisson distributed sequences have the number variance $\Sigma^2(L) = L$ and the rigidity $\Delta_3(L) = L/15$. The results of random matrix theory for the number variance of GOE- and GUE-distributed sequences are given by [88]

$$\begin{aligned} \Sigma^2(L) &= \frac{2}{\pi^2} \left\{ \log(2\pi L) + \gamma + 1 + \frac{1}{2} \mathrm{Si}^2(\pi L) - \frac{\pi}{2} \mathrm{Si}(\pi L) \right. \\ &\quad \left. - \cos(2\pi L) - \mathrm{Ci}(2\pi L) + \pi^2 L \left[1 - \frac{2}{\pi} \mathrm{Si}(2\pi L) \right] \right\} \quad , \end{aligned} \tag{158}$$

and

$$\Sigma^2(L) = \frac{1}{\pi^2} \left\{ \log(2\pi L) + \gamma + 1 - \cos(2\pi L) - \mathrm{Ci}(2\pi L) + \pi^2 L \left[1 - \frac{2}{\pi} \mathrm{Si}(2\pi L) \right] \right\} \quad , \tag{159}$$

respectively. Results for the spectral rigidity follow from eq. (126).

Berry developed a semiclassical theory which predicts, for what values of the parameter L both statistics show universal behaviour, and for what values of L there is a departure from universality. The derivation of this theory is based on Gutzwiller's semiclassical expression for the density of states as a sum over periodic orbits. Here we discuss the theory for the spectral rigidity, but the argumentation is analogous for the number variance.

Berry's theory considers three ranges of the parameter L:

For very small values $L \ll 1$ the rigidity approaches $\Delta_3(L) \to L/15$, which is a consequence of the fact that $N'(E')$ is a staircase. In terms of the periodic-orbit sum the same result can be obtained with the use of a semiclassical sum rule. This sum rule is derived on the assumption that Gutzwiller's periodic-orbit sum is conditionally convergent and results in a series of δ-functions. The fact that the very long orbits are responsible for the δ-peaks, which must be distributed along the real energy axis with the right mean density, leads to constraints for the amplitudes and phases of the periodic orbits in the trace formula. These constraints give rise to the sum rule mentioned above.

The second range of the parameter L is given by $1 \ll L \ll L_{max}$, where L_{max} is the quotient between the largest energy scale $(\Delta E)_{max}$ in the periodic-orbit sum and the mean energy level

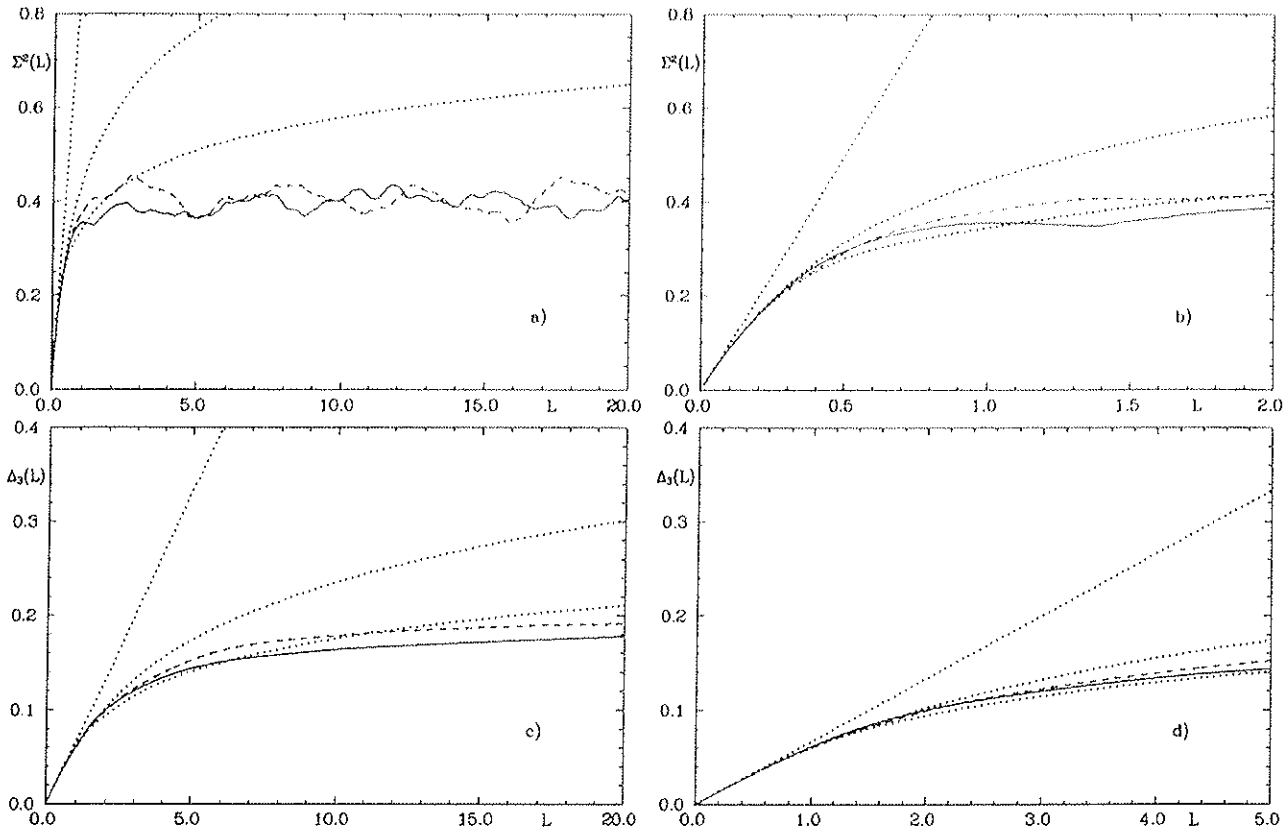

Figure 15: The number variance $\Sigma^2(L)$, a) and b), and the spectral rigidity $\Delta_3(L)$, c) and d). Full lines: results for even energy eigenfunctions, dashed lines: results for odd energy eigenfunctions, dotted lines: in the sequence of increasing functional values: the results for GUE-, GOE- and Poisson distributed sequences.

distance $1/\bar{d}(E)$. $(\Delta E)_{max}$ is the energy range within which the oscillatory contribution of the shortest orbit in the periodic-orbit sum oscillates once: $(\Delta E)_{max} = 2\pi\hbar/T_{min}$. Here T_{min} denotes the period of the shortest periodic orbit. In the considered intermediate range of the parameter L the behaviour of the rigidity is determined mainly by the contributions of orbits to the periodic-orbit sum, whose lengths are in an intermediate range, too. It is assumed that they are large enough in order that the orbits are uniformly distributed in phase space. On the other hand they must be small enough, so that pairs of orbits with an action difference smaller than $\hbar$ occur rarely. On this assumption a classical sum rule is obtained, which is a consequence of the exponential proliferation of long orbits and the uniformity of exploration of phase space by long orbits. Using this sum rule it is shown that the rigidity agrees with the random matrix predictions in the considered range of the parameter L.

Within the third range $L \gg L_{max}$ the properties of the rigidity are determined by the contributions of the very short orbits to the trace formula. These orbits have non-universal properties, which differ from system to system. As a consequence of the fact that there is a shortest orbit the rigidity saturates and approaches a non-universal constant Δ_∞ as $L \to \infty$.

In figure 15 the number variance and the spectral rigidity are shown for the hyperbola billiard. The GOE expectation is met only for very small values of the parameter L. The

number variance $\Sigma^2(L)$ deviates from the GOE curve already at $L \approx 0.4$, and in case of the spectral rigidity $\Delta_3(L)$ the deviation occurs at $L \approx 2.0$. These values of L are much smaller than the values that would be expected from Berry's theory. With the length of the shortest periodic orbit $l_{min} = 2.0$ the value of L_{max} at energy $E = 800$ is given by

$$L_{max} = 4\pi\sqrt{E}\,\bar{d}(E)/l_{min} \approx 37 \tag{160}$$

for both symmetry subspaces. The reason for the disagreement with the predictions of Berry's theory is the fact, that the special properties of the hyperbola billiard prevent Berry's theory from being applicable to this system. One crucial assumption for the derivation of universality is the uniformity of exploration of phase space by long orbits. The hyperbola billiard has a phase space of infinite volume and for that reason it cannot be covered uniformly by a finite number of orbits. Still it would be favourable to understand the properties of the rigidity and the number variance on basis of the periodic orbits of the system. This requires a detailed examination of the validity of the assumptions of Berry's theory in case of the hyperbola billiard and possible replacements of this assumptions.

Both considered statistics show, however, a saturation as is predicted by Berry's theory, and they saturate already for very small values of the parameter L. In most systems the saturation occurs only for large values of the parameter L. The determination of the saturation values of $\Sigma^2(L)$ and $\Delta_3(L)$ then requires the knowledge of a large number of energy eigenvalues, which for most systems are not available. In figure 15 a) $\Sigma^2(L)$ saturates very early and then oscillates around the value $\Sigma_\infty \approx 0.40$ for the eigenvalues of even wavefunctions as well as for the eigenvalues of odd wavefunctions. The rigidity saturates at larger values of L. At $L = 20$ the values of $\Delta_3(L)$ are still slightly increasing. In order to obtain the saturation value Δ_∞ for the two curves, a fit with functions of the form

$$\Delta_3(L) = \Delta_\infty \left(1 + \frac{a}{L} + \frac{b}{L^2}\right) \quad , L \gg 1 \ , \tag{161}$$

is made. The result is the value $\Delta_\infty \approx 0.20$ for both cases.

Theoretically a relation between Δ_∞ and Σ_∞ follows from eq. (126). $\Delta_3(L)$ is replaced for large values of L by eq. (161) and eq. (126) is differentiated four times with respect to L. This results in a differential equation for $\Sigma^2(L)$ for large values of L [39]. This differential equation implies

$$\Sigma^2(L) = 2\Delta_\infty + O(L^{-3}) \quad , L \to \infty \ , \tag{162}$$

so that $\Sigma_\infty = 2\Delta_\infty$, which is verified by the numerically obtained values. In addition eq. (162) gives an explanation for the fact, that $\Sigma^2(L)$ saturates much faster than $\Delta_3(L)$. Correction terms to the saturation value are of order $O(L^{-3})$ for large values of L, whereas in case of the rigidity correction terms of order $O(L^{-1})$ are obtained.

V Numerical Examination of the Periodic-Orbit Theory

The Gutzwiller trace formula allows the determination of quantum mechanical energies of classically chaotic systems in the limit $h \to 0$ by making use only of classical quantities. It has, however, scarcely been used for the determination of energies. This is due to several theoretical and practical problems, which are connected with the trace formula.

One problem is the sum over an infinite number of periodic orbits and the question of its convergence, as has been discussed in chapter II. Due to the exponential proliferation of the periodic orbits a positive imaginary part must be given to the energy E in order that the periodic-orbit sum converges absolutely. The lower limit for $\mathrm{Im}\, E$ depends on the topological entropy, which is a measure for the exponential increase of the number of orbits, and the asymptotic instability of orbits in the limit that the lengths of the trajectories go to infinity (see eq. (77)). The fact of a finite (positive) lower limit for $\mathrm{Im}\, E$ prevents the determination of the energies by an absolutely convergent periodic-orbit sum. If this sum moreover is not conditionally convergent for real values of the energy E, the trace formula has to be smoothed with suitable test functions as was done in chapter II. As consequence of the smoothing the poles at the energies are replaced by peaks of finite height and width. This does not restrict the accuracy for the determination of the energies, if the width of the peaks can be made arbitrarily small. Whether this can be done depends on the kind of smoothing, which is chosen. If the peaks have the form of Breit-Wigner curves, they must have a minimum width in order that the periodic-orbit sum converges absolutely. In case of a Gaussian smoothing there is no such restriction for the width of the peaks, so that a Gaussian smoothed trace formula allows the determination of the energies with arbitrary accuracy. In the latter case one still has a sum over an infinite number of periodic orbits. Most orbits, however, give a negligible contribution to the periodic-orbit sum, so that the determination of energies with a finite resolution requires the sum over a finite number of orbits only.

A further question is, what the effect of the semiclassical approximations is, that were used in the derivation of the trace formula. There is no estimation for the size of the error of these approximations. The trace formula defines a function, which is an approximation to the trace of the Green function in those parts of the complex E-plane, in which the periodic-orbit sum converges. Let us assume that this function in principle can be defined in parts of the complex E-plane, where the sum diverges, by analytical continuation. Then it is assumed that this semiclassical approximation to the trace $g(E)$ of the Green function has poles at values of E, which are close to the energy eigenvalues of the Hamiltonian operator. But what the actual relationship is between the pole structure of $g(E)$ and its approximation is not known. For this reason it is not clear, for example, if the Gaussian peaks actually converge into a series of delta-functions, if the width of the peaks is made smaller and smaller. There are only few numerical tests of the periodic-orbit theory, and there is no detailed quantitative analysis of the accuracy of the trace formula.

The reason for this is the high numerical effort, that an evaluation of the trace formula requires. In chaotic systems it is very difficult to determine a fairly large number of periodic orbits with sufficient accuracy, as has been discussed at the beginning of chapter III. It is even more difficult to determine a complete spectrum of the shortest orbits, whose actions are smaller than a given value. On the other hand the evaluation of the trace formula requires

the knowledge of a very large number of the shortest orbits, if one wants to determine more than the first few energies. A rough estimate for the order of magnitude of the number of orbits that are needed in order to resolve two adjacent energies, which are separated by an energy difference ΔE, is obtained by observing that every orbit contributes a term to the periodic-orbit sum, which oscillates as a function of E (see eq.(34) or the smoothed trace formulae of this chapter). In order to resolve ΔE one has to include in the periodic-orbit sum at least all the shortest orbits up to those, whose contribution oscillates once as E is changed by ΔE. For small ΔE this leads to the condition $\mathrm{d}S(E)/\mathrm{d}E = T(E) \approx 2\pi\hbar/\Delta E$, where $T(E)$ is the period of an orbit with energy E. Because of the exponential proliferation of the number of orbits, the resolution of the energy interval $\Delta E/2$ requires the summation over the square of the number of orbits, which are needed for the resolution of ΔE. For this reason soon a limit for the energy resolution is reached in practice.

The fact that for many chaotic systems only a relatively small number of orbits is known is also the reason why in many papers not a smoothed trace formula is used, but the original (divergent) formula, which is truncated. One often finds that the truncated trace formula gives good results for the determination of the first few energies. But this effect is only expected, if not too many orbits are taken into account. If the sum extends over more and more orbits, it is expected that the effect of the divergence of the periodic-orbit sum shows up in the form of wild oscillations, which finally prevent a discrimination of the energies. This does not happen in case of a Gaussian smoothed trace formula, for example. In addition, the smoothing parameter can be chosen small enough, so that the smoothing does not give rise to a decrease of the energy resolution.

It is of strong interest to know what the properties of the periodic-orbit theory as approximative theory actually are. A further point is that almost all the semiclassical theories for chaotic systems use the same kind of approximation methods, that is stationary phase approximations, whether it is the Gutzwiller trace formula or the approximation to the energy eigenfunctions [23] or to the Wigner function [26] or the new quantization method of Bogomolny [16]. For example, in deriving the trace formula a stationary phase approximation is used three times. It is therefore of interest to see, what the effects of these approximations are for one example, for which the trace formula is not exact.

For the reasons already stated the hyperbola billiard gives the possibility to do such examinations. In order to test the trace formula quantitatively it is of importance to use the smoothed trace formula, since in this way one has control over the error that one makes by summing over a finite number of orbits only. In case of the unsmoothed trace formula there is no estimation for this error. By using a Gaussian smoothing, for example, the smoothing parameter can be chosen in such a way, that the sum of the contributions of the infinite number of orbits, which are neglected in the periodic-orbit sum, is small in comparison with the contribution of the shortest orbits, over which the sum is taken. It is even possible to do the periodic-orbit sum exactly. This can be done by choosing the smoothing function $h(p)$ in eq. (84) in such a way that its Fourier cosine transform $g(x)$ is equal to zero, if its argument x is larger than a certain value. In this case the periodic-orbit sum contains a finite number of orbits.

In this chapter the trace formula is evaluated for several examples of the smoothing function $h(p)$. Energies are determined and the accuracy of the trace formula is analyzed. At the end of this chapter the Riemann-Siegel analogue of Berry and Keating is examined and the results are compared to the results for the smoothed trace formulae.

V.1 The Generalized Periodic-Orbit Sum Rules for the Hyperbola Billiard

The basic formula that is used throughout this chapter is given by eq. (84), which is applied to the energy eigenvalues of even and odd wavefunctions of the hyperbola billiard, respectively. This is equivalent to the application of eq. (84) to the desymmetrized hyperbola billiard with Neumann and Dirichlet boundary conditions, respectively, on the line $y = x$, and Dirichlet boundary conditions on the remaining part of the boundary. Again dimensionless units are used with $\hbar = 1 = 2m$, where m is the mass of the particle. Eq. (84) then has the form

$$\sum_n h(p_n) \approx 2 \int_0^\infty \mathrm{d}p\, p\, h(p) \bar{d}(E = p^2) + \sum_\gamma \sum_{k=1}^\infty \frac{l_\gamma\, \chi_\gamma^k\, g(k l_\gamma)\, a_{\gamma,k}}{\exp(k u_\gamma/2) - (-1)^{k n_\gamma} \exp(-k u_\gamma/2)} \quad . \tag{163}$$

$\chi_\gamma = (-1)^{\bar{n}_\gamma}$, where $\bar{n}_\gamma$ is the number of reflections on those parts of the boundary, where Dirichlet boundary conditions are required. n_γ is the total number of reflections on the boundary during one traversal of the periodic orbit γ. Every orbit whose code word contains an odd number of "$-$" corresponds to an orbit in the full hyperbola billiard, which has double length and is symmetric under reflection on the line $y = x$. For that reason the number of reflections on the line $y = x$ must be odd. An orbit whose code word contains an even number of "$-$" corresponds to an orbit in the full hyperbola billiard which has the same length, and for that reason the number of its reflections on the line $y = x$ must be even. In addition every "+" and every "$-$" corresponds to an even number and every "0" to an odd number of reflections on the remaining part of the boundary, i. e. the boundary along the hyperbola $y = 1/x$ and the x-axis. It follows that

$$n_\gamma = (n_{0,\gamma} + n_{-,\gamma}) \bmod 2 \quad , \tag{164}$$

where $n_{0,\gamma}$ and $n_{-,\gamma}$ are the numbers of "0" and "$-$", respectively, in the code word of the orbit γ.

Neumann boundary conditions along the line $y = x$:
From the considerations above it follows that

$$\bar{n}_\gamma = n_{0,\gamma} \bmod 2 \quad . \tag{165}$$

The mean energy density is

$$\bar{d}(E) = \frac{\mathrm{d}}{\mathrm{d}E} \bar{N}^+(E) \quad , \tag{166}$$

and $\bar{N}^+(E)$ is given by eq. (144). Further from eq. (55) one obtains

$$a_{\gamma,k} = a^+_{\gamma,k} = \begin{cases} (1 + (-1)^k e^{-k u_\gamma})^{-1} & \text{for the orbit with code word } a = (\mathrm{b}) \\ 1 & \text{otherwise} \quad . \end{cases} \tag{167}$$

Dirichlet boundary conditions along the line $y = x$:

In this case

$$\bar{n}_\gamma = n_\gamma \tag{168}$$

and

$$\bar{d}(E) = \frac{\mathrm{d}}{\mathrm{d}E} \bar{N}^-(E) \quad , \tag{169}$$

where $\bar{N}^-(E)$ is given by eq. (144). Further from eq. (56) one obtains

$$a_{\gamma,k} = a_{\gamma,k}^- \cdot \begin{cases} (1 + (-1)^k e^{k\omega_\gamma})^{-1} & \text{for the orbit with code word } a = (\mathrm{b}) \\ 1 & \text{otherwise} \end{cases} . \tag{170}$$

V.2 The Unsmoothed Energy Density

Eq. (77) is a condition for the imaginary part of the momentum $p = \sqrt{E}$, for which the periodic-orbit sum for the trace of the Green function $g(E)$ is absolutely convergent. However, the orbits contribute with different signs to the periodic-orbit sum. As will be seen below the number of orbits, which give a positive contribution to the sum is of the same order of magnitude as the number of orbits, whose contribution is negative. For that reason it can be expected that the region of conditional convergence of the periodic-orbit sum in the complex p-plane approaches much closer the axis of real momentum p than the region of absolute convergence. The question, whether the evaluation of the periodic-orbit sum on the real p-axis gives any sensible results, is examined numerically.

The numerical evaluation is done for the unsmoothed energy density $d(E)$ which is related to the trace of the Green function $g(E)$ by eq. (18). Its periodic-orbit approximation is real for real values of the energy E and it can be obtained formally by choosing the smoothing function $h(p')$ to be a delta-function

$$h(p') = \delta(p^2 - p'^2) . \tag{171}$$

Then

$$g(x) = \frac{1}{2\pi|p|} \cos(px) . \tag{172}$$

Of course this function $h(p')$ does not obey the conditions, which guarantee absolute convergence of the periodic-orbit sum.

The results of a numerical evaluation of the trace formula for even and odd wavefunctions are shown in figure 16 a) and b), respectively. The periodic-orbit sum is taken over all orbits that have been determined, that is all orbits with code lengths $N \leq 14$ or length $l_\gamma \leq 20$, which are 533 760 orbits altogether. The limit of the k-summation is given by $kl_\gamma \leq 40$. The positions of the energies E_n are marked by triangles. Figure 16 shows distinct peaks at the energies E_n, if neighbouring energies are separated well enough. In the following E_n^+ denotes the n-th eigenvalue of even wavefunctions. The corresponding notation for the eigenvalues of odd wavefunctions is E_n^-.

In figure 16 a) the first 15 energies with exception of the two adjacent energies E_8^+ and E_9^+ can be resolved. E_8^+ and E_9^+ are separated by a momentum difference $\Delta p \approx 0.169$. The resolution of this momentum difference requires at least the summation over orbits with a length below $l = \Delta p/2\pi \approx 37.2$. The mean value of lengths with code length $N = 14$ is $\bar{l}_{14} \approx 28.4$. As a consequence the orbits over which the periodic-orbit sum is taken are not sufficient for the resolution of two different peaks. Only one peak for both energies can be seen in figure 16. The momentum difference between the energies E_{16}^+ and E_{17}^+ is equal to $\Delta p \approx 0.178$, which corresponds to a length of $l \approx 35.3$. But in this case two different peaks can be seen, although the height of the second peak is distinctly smaller than the first peak. The momentum difference between the maxima of the two peaks in the figure is, however, larger than the momentum difference between the corresponding two energy eigenvalues. It

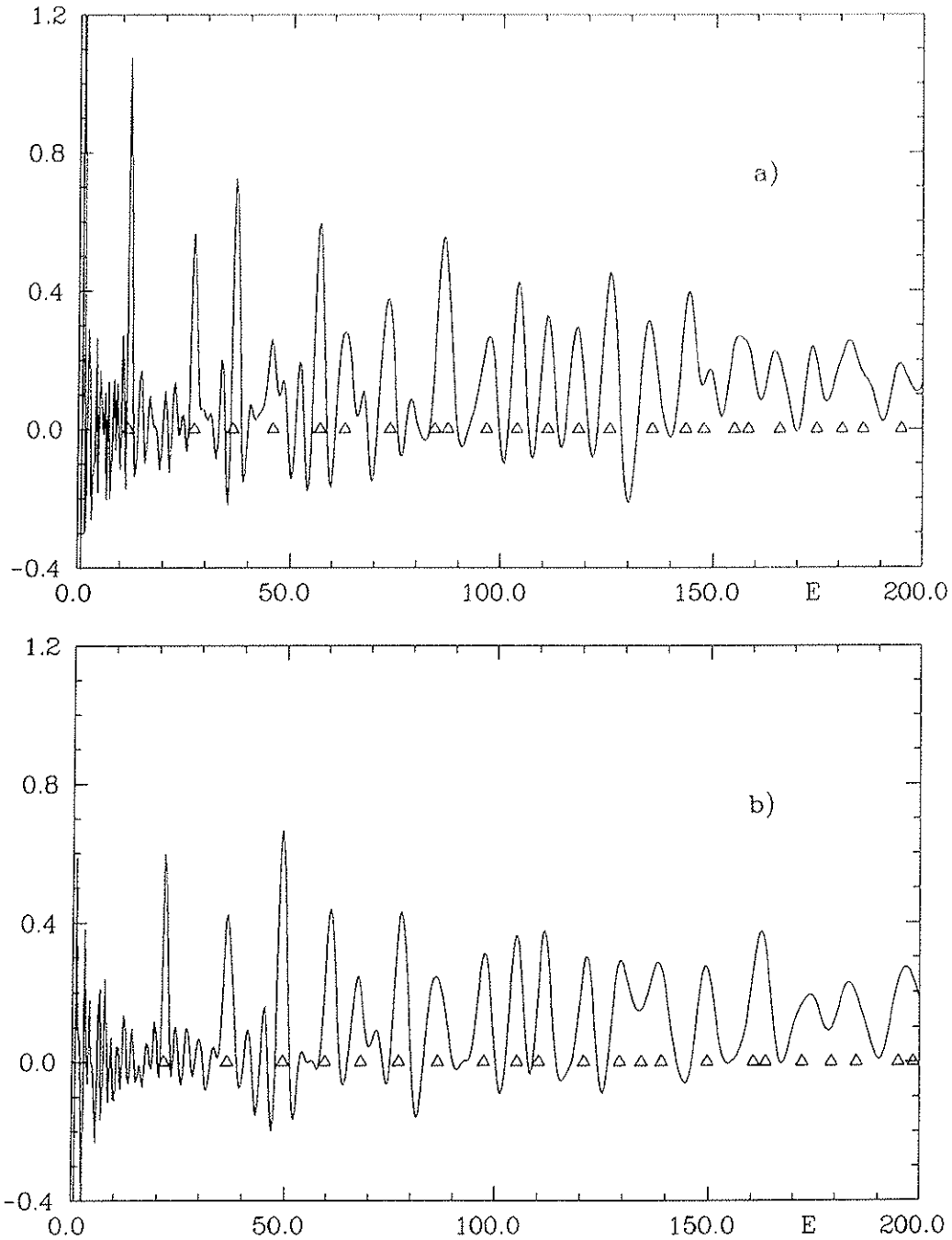

Figure 16: The results of an evaluation of the trace formula for the unsmoothed level density for the energy eigenvalues of a) even and b) odd wave functions. The triangles mark the positions of the energy eigenvalues. The sum is taken over all periodic orbits, which have a length below $l = 20$ or a code length $N \leq 14$.

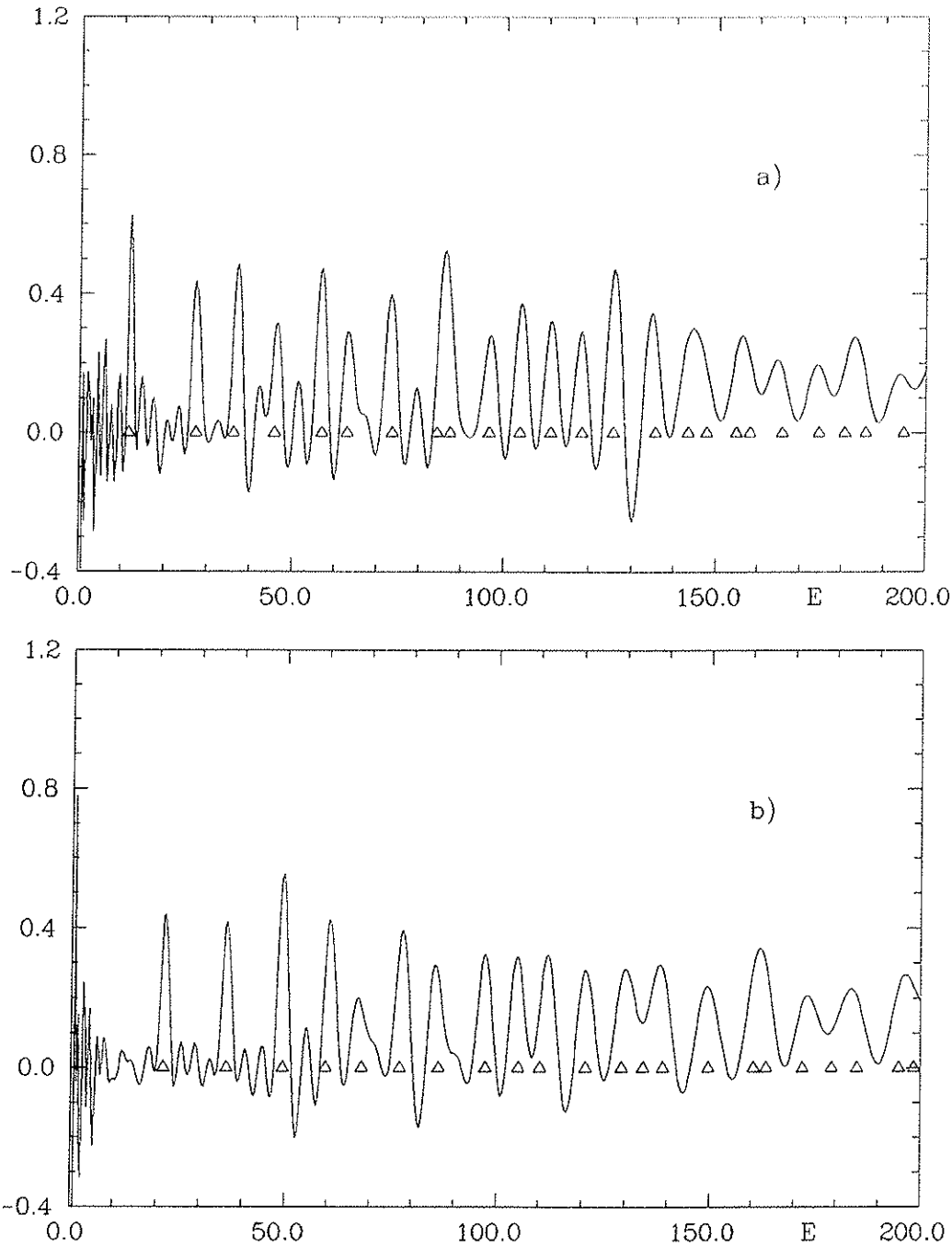

Figure 17: The results of an evaluation of the trace formula for the unsmoothed level density for the energy eigenvalues of a) even and b) odd wave functions. The triangles mark the positions of the energy eigenvalues. The sum is taken over all periodic orbits, which have a length below $l = 20$.

is $\Delta p \approx 0.209$, which corresponds to $l \approx 30.1$. This can be interpreted as the start of the splitting of one peak into two. As more and more lengths are included in the sum it is expected that the second peak increases, and that probably both peaks move closer together.

In case of the eigenvalues of odd wavefunctions the first 11 energies can be resolved. The next energies E_{12}^-, E_{13}^- and E_{14} are separated by momentum differences of $\Delta p \approx 0.220$ and $\Delta p \approx 0.198$, respectively. The corresponding lengths, up to which the periodic-orbit sum has to be taken in order to resolve these momentum differences are given by $l \approx 28.6$ and $l \approx 31.8$, respectively. For this reason there are only two peaks for the three energies.

The result of this numerical investigation of the unsmoothed energy density is, that the application of the periodic-orbit theory for this quantity gives good results. There can be different reasons for this. First it is possible that the periodic-orbit sum is conditionally convergent for real values of the momentum p. The trace formula then gives a semiclassical approximation for the level density with peaks at approximations to the energy eigenvalues, although those peaks need not be delta-peaks. Second it is possible that the periodic-orbit sum is divergent. The good results shown in figure 16 are then due to the fact that not too many orbits have been included in the periodic-orbit sum. If more and more orbits are included in the sum, it then is expected that oscillations arise between the peaks at the energies, which gradually increase, so that finally the peaks disappear in the background.

In order to get an impression how the curve for the approximated energy density changes as a different number of orbits is included in the periodic-orbit sum, figures 17 a) and b) show the result of an evaluation of the periodic-orbit sum with all orbits that have a length below $l = 20$. Although the number of orbits is very much less than the number of orbits that have been used for figures 16 a) and b), 13 098 orbits in comparison with 533 760 orbits, the number of peaks that can be resolved is almost the same in both cases. The reason for this is that the momentum differences between an energy, that can be resolved in figure 16, and its neighbouring energies are in most cases so large that the orbits with length up to $l = 20$ are sufficient for the resolution of this energy. One difference between figures 16 a) and 17 a) is that in 17 a) there is no beginning splitting of the peak for the energies E_{16}^+ and E_{17}^+ into two peaks. In figure 17 b) the two energies E_9^- and E_{10}^- can be resolved although their momentum difference is equal to $\Delta p = 0.245$ which corresponds to $l = 25.6$, so that a summation over all orbits with length below $l = 20$ seems not to be enough for the resolution of these peaks. However, for the two corresponding peaks in figure 17 b) one has $\Delta p = 0.344$ and $l = 18.3$. The resolution of two different peaks therefore is probably due to the fact that the semiclassical approximations for the two energies E_9^- and E_{10}^- have a larger separation than the actual energies. If more orbits are included the peaks move slightly together and in figure 16 b) the difference is equal to $\Delta p = 0.313$. Although most of the peaks are improved, if more orbits are included in the periodic-orbit sum, there are peaks, which in the second pair of figures are better than in the first pair of figures. These are the peaks at the energies E_4^+ and E_7^-. However, one has to be cautious with an interpretation of this result as a possible sign of a divergence, since the orbits are only complete up to the length $l = 20$.

A further examination of the change of the curve for the energy density as more orbits are included in the periodic-orbit sum is carried out by a consideration of the contributions of orbits within different ranges of the code length N. Figure 18 shows the results of an evaluation of the trace formula with all orbits with $1 \leq N \leq 7$ and $8 \leq N \leq 14$, respectively, for the eigenvalues of even and odd wavefunctions. The curves are discussed for the even case, but qualitatively the same statements can be made for the odd case. In figure 18 a)

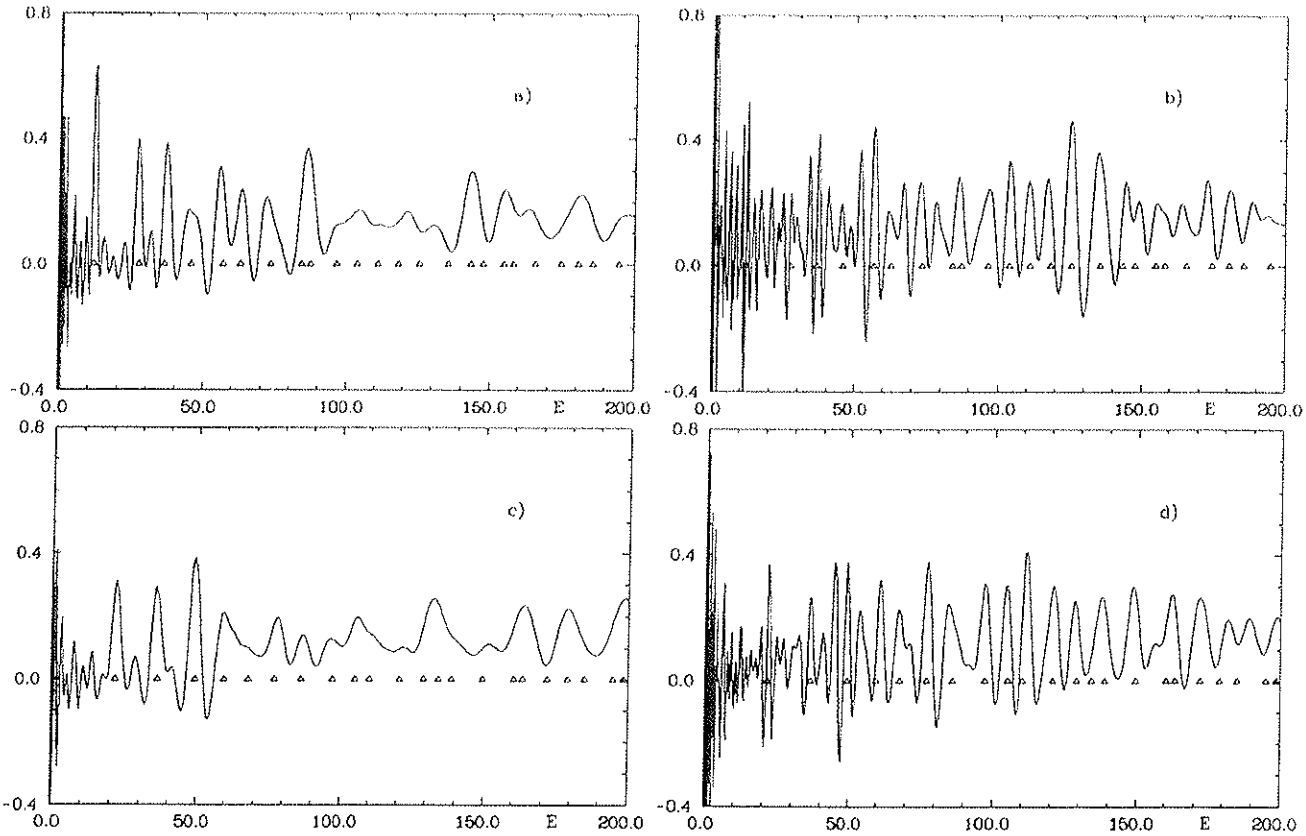

Figure 18: The results of partial sums over periodic orbits in the trace formula for the energy density. a) and b) show the results of a summation over all orbits with code length $1 < N < 7$ and $8 < N < 14$, respectively, for the energy eigenvalues of even wavefunctions. c) and d) show the corresponding results for energy eigenvalues of odd wavefunctions.

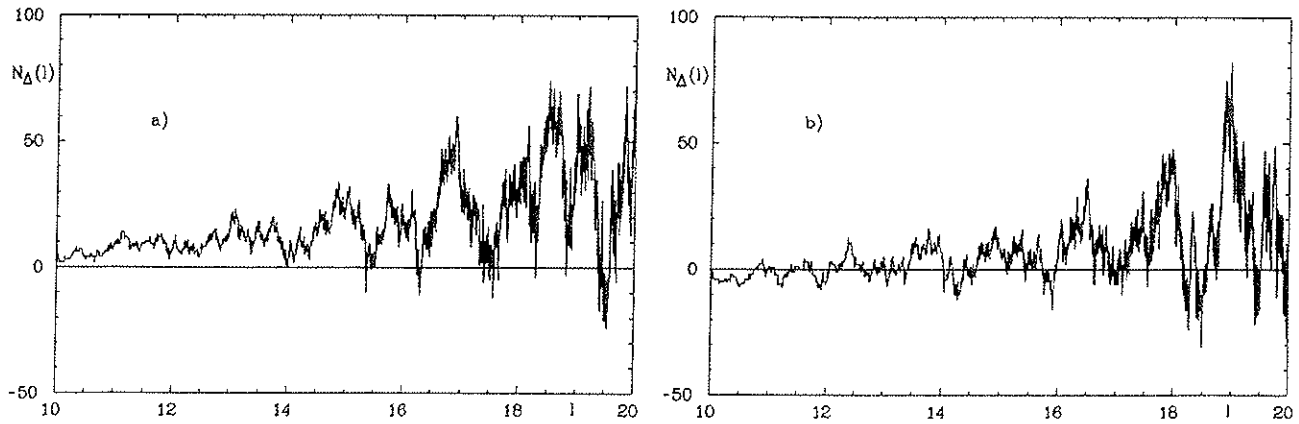

Figure 19: The difference $\mathcal{N}_\Delta(l)$ of the numbers of orbits, which contribute to the periodic-orbit sum with a phase factor $\chi_\gamma^k = +1$ and $\chi_\gamma^k = -1$, respectively, for the a) even and b) odd case.

the first seven peaks can be resolved. For higher energies the curve can be interpreted as a superposition of peaks at the energy eigenvalues, so that the curve can be understood qualitatively over the entire considered energy range. In figure 18 b) there are pronounced peaks also at the higher energies E_{10}^{+} - E_{15}^{+}. In lower energy range there are oscillations, which have maxima at the energies E_1^{+} - E_7^{+}, so that the longer periodic orbits also produce an increase of the peaks at low energies. However, the oscillations between the low energies partly have the same amplitude as the peaks at the energies. In case of the energy E_4^{+} the amplitudes on one side are even higher.

In order to get a better estimation of the convergence properties of the periodic-orbit sum the following quantity is defined

$$\begin{aligned} \mathcal{N}_\Delta(l) \;:=\; & \#\{\text{periodic orbits } \gamma \text{ with } l_\gamma \leq l \text{ and } \chi_\gamma^k = +1\} - \\ & \#\{\text{periodic orbits } \gamma \text{ with } l_\gamma \leq l \text{ and } \chi_\gamma^k = -1\} \;. \end{aligned} \tag{173}$$

Here the total number of periodic orbits is considered, not only the primitive periodic orbits. $\mathcal{N}_\Delta(l)$ is different in the even and the odd case, because of the different phase factors χ_γ. The periodic orbits contribute with different signs to the periodic-orbit sum. The sign depends on the phase factor χ_γ^k and the phase of the cosine-function in eq. (172). If the periodic-orbit sum is evaluated at a fixed value of the momentum p then for large lengths there will be a great number of orbits within one half-period of the cosine-function because of the exponential proliferation of the number of periodic orbits. The mean Lyapunov exponent is for orbits with different values of the phase factor χ_γ^k to a good approximation the same. The change of the function $\mathcal{N}_\Delta(l)$ therefore indicates what the contribution of one half-period of the cosine-function to the periodic-orbit sum is, and thus it allows a better estimation of the convergence properties of the orbit sum. In figure 19 the function $\mathcal{N}_\Delta(l)$ is shown for the even and odd case in the range $0 < l < 20$ where all orbits are known. The function oscillates and its mean increase is very low in comparison with the increase of the total number of orbits which is shown in figure 8. From this one can conclude that the region of conditional convergence reaches up much closer to the real momentum axis than the region of absolute convergence. Possibly the periodic-orbit sum is even convergent for real values of the momentum p.

V.3 The Breit-Wigner Smoothed Energy Density

If the periodic-orbit sum is not convergent, the level density has to be smoothed in order to obtain a convergent sum. A natural kind of smoothing is carried out by giving the momentum p a constant imaginary part $i\alpha/2$ before taking the imaginary part of the periodic-orbit sum for the trace of the Green function $g(E)$. The result is a smoothed energy density, which consists of a superposition of Breit-Wigner curves, that are centered at the quantum mechanical energies. The smoothing function is given by

$$h(p') = \frac{\alpha^2 p^2}{(p^2 - p'^2)^2 + \alpha^2 p^2} \tag{174}$$

It is normalized such that the height at the maximum is equal to one. The Fourier cosine transform of $h(p')$ is equal to

$$g(x) = \frac{\alpha p}{2(p^4+\alpha^2p^2)^{1/4}}\cos\{x\sqrt{\frac{1}{2}(\sqrt{p^4+\alpha^2p^2}+p^2)} - \frac{1}{2}\arctan\frac{\alpha}{p}\}$$
$$\times\exp\{-x\sqrt{\frac{1}{2}(\sqrt{p^4+\alpha^2p^2}-p^2)}\} \quad . \tag{175}$$

The width of the Breit-Wigner curves is energy-dependent, and the condition for the absolute convergence of the periodic-orbit sum is a condition for the parameter α. It is $\alpha > 2\sigma$, where σ is given in eq. (77). Even if the periodic-orbit sum is convergent, it is of use to consider a smoothed energy density. The reason for this is that the numerical evaluation is done with a finite number of orbits. The maximum length l of these orbits sets a lower limit for the momentum difference $\Delta p = 2\pi/l$, which can be resolved. By using a smoothed trace formula with a smoothing parameter α the attainable momentum resolution is limited by the finite width of the peaks at the energies. If one chooses α in such a way that both lower limits for Δp are the same, then the resolution is not diminished by using a smoothed trace formula. But the periodic-orbit sum of the smoothed level density has improved convergence properties because of the exponential damping factor in eq. (175). A relation between Δp and α is obtained by requiring that between two energies the level density falls off to half of its value at the energies levels, if the energies are separated by Δp. This leads to the condition

$$1+\frac{\alpha^2p^2}{(\Delta p)^2(2p+\Delta p)^2+\alpha^2p^2} = 4\frac{\alpha^2p^2}{(\Delta p)^2/4(2p+\Delta p/2)^2+\alpha^2p^2} \quad , \tag{176}$$

which for $\Delta p \ll p$ results in

$$\alpha = \Delta p\left(\frac{5+\sqrt{33}}{4}\right)^{-1/2} \approx \Delta p/1.64 \quad . \tag{177}$$

In practical calculations there is some difficulty in the estimation of the minimal Δp, that can be resolved with a finite number of orbits. Normally the periodic orbits, that are used for the evaluation of the trace formula, are not complete up to the maximum length of the orbits. For that reason Δp is not necessarily determined by the maximum length, but by some smaller length. In figure 20 the Breit-Wigner smoothed energy density is shown for the energy eigenvalues of even and odd wavefunctions, respectively. The parameter α is chosen to be $\alpha = 0.15$, which corresponds to $\Delta p \approx 0.25$. The dashed curve is calculated from the quantum mechanical energy spectrum. Both curves agree well in their main features over the whole energy range. In comparison with the approximation for the unsmoothed level density the oscillations between the peaks are suppressed. This allows a better discrimination of the peaks at the energy eigenvalues. For example the peaks at the energies E_4^+, E_6^+ and E_5^- now are more distinct. As a consequence of the smoothing the maxima of the peaks are slightly shifted, as can be seen in tables 8 and 10 at the end of this chapter.

Most of the peaks of the curve, that is obtained from the periodic-orbit sum, have a smaller height than the peaks of the dashed curve. The reason for this are the missing contributions of orbits, which are neglected in the periodic-orbit sum, that is orbits with code length $N > 14$ and length $l_\gamma > 20$. The contributions of these orbits can be diminished by increasing the smoothing parameter α. The requirement that the contributions of orbits,

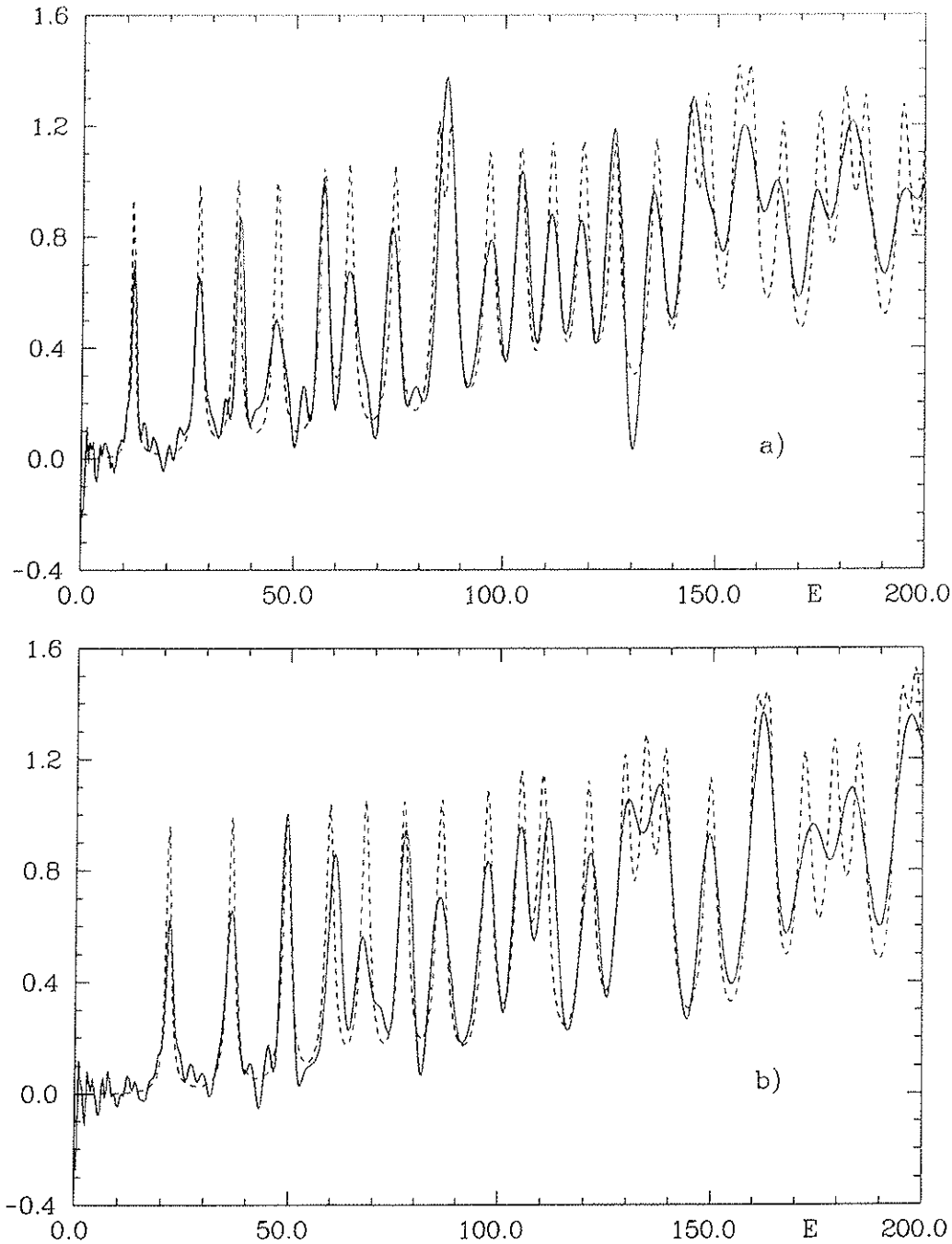

Figure 20: The Breit-Wigner smoothed level density calculated from the periodic-orbit theory (full line) and the quantum mechanical energy spectrum (dashed line) for the energy eigenvalues of a) even and b) odd wavefunctions. The smoothing parameter is equal to $\alpha = 0.15$.

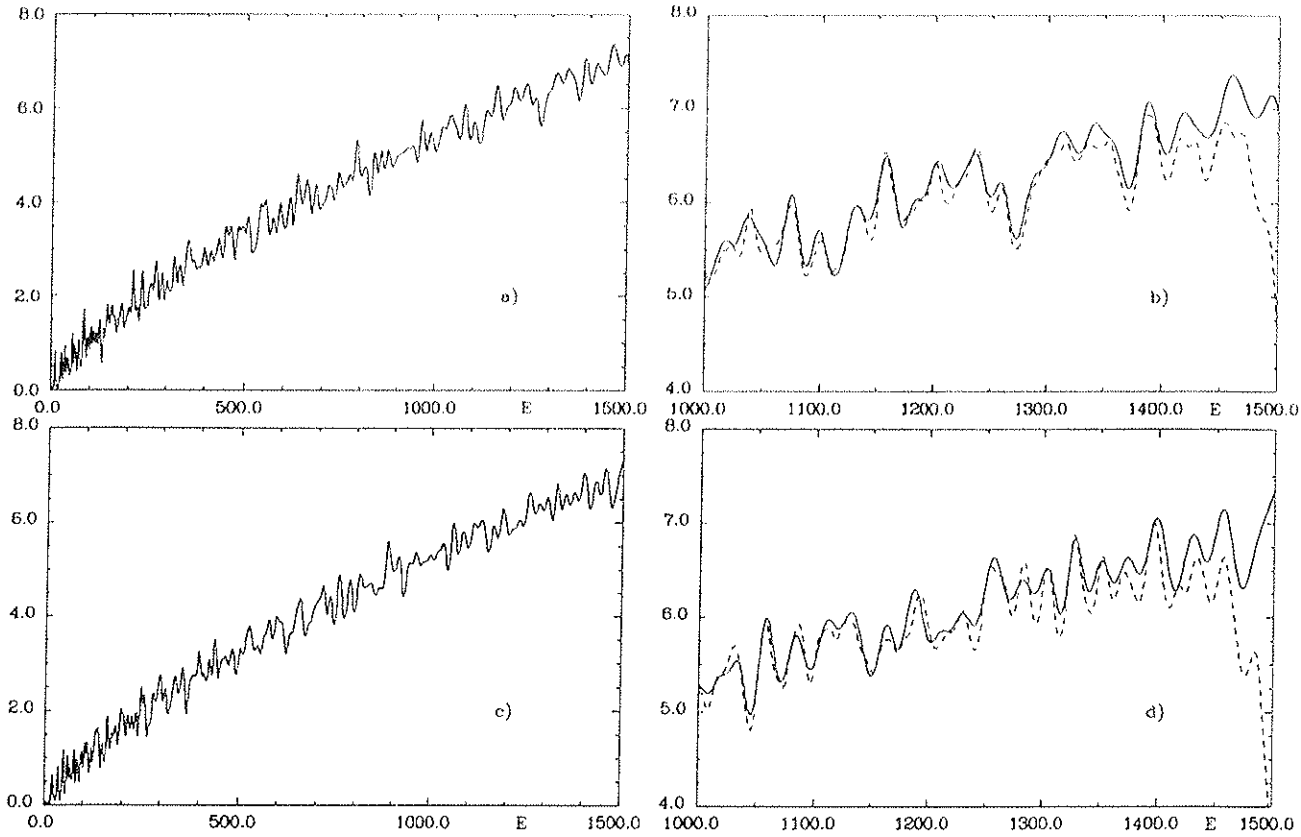

Figure 21: The periodic-orbit approximation for the Breit-Wigner smoothed level density with $\alpha = 0.25$ for the eigenvalues of a) even and c) odd wavefunctions. b) and d) show a section of a) and c), respectively, in comparison with corresponding curves, that are obtained from the quantum mechanical energy spectrum (dashed line).

which are neglected, is not significant gives a condition for α. However, the estimation of the value of α which is determined by this condition is difficult, because the orbits contribute with different phase factors to the sum. In figure 21 an evaluation of the Breit-Wigner smoothed trace formula is shown for $\alpha = 0.25$. Figures 21 a) and c) show the results for the energy range $0 < E < 1500$. In figures 21 b) and d) the curves, that are obtained from the periodic-orbit theory, are compared to curves, which are computed with the numerically determined energy eigenvalues, in the range $1000 < E < 1500$. As can be seen there also is a good agreement between corresponding curves in the range of higher energies. Close to the energy $E = 1500$ the dashed curves fall off because of the missing contributions of the energy eigenvalues above $E = 1500$.

A disadvantage of the Breit-Wigner smoothing is the fact, that in general the smoothing parameter α cannot be chosen arbitrarily. If the trace formula for the level density is divergent, then α has to be above a certain minimal value in order that the Breit-Wigner smoothed periodic-orbit sum converges. This sets a limit for the energy resolution, which can be attained in principle, even if an arbitrary number of periodic orbits is available. A kind of smoothing which is free of such a limitation is the Gaussian smoothing, which is discussed in the following section.

V.4 The Gaussian Smoothed Energy Density

The Gaussian smoothed level density has peaks in form of Gaussian curves at the energy eigenvalues. It is obtained, by choosing the smoothing function to be

$$h(p') = \exp\{-\frac{(p-p')^2}{\varepsilon^2}\} + \exp\{-\frac{(p+p')^2}{\varepsilon^2}\} \ . \tag{178}$$

Then

$$g(x) = \frac{\varepsilon}{\sqrt{\pi}} \cos(px) \exp\{-\frac{\varepsilon^2 x^2}{4}\} \ . \tag{179}$$

The periodic-orbit sum is absolutely convergent for every positive value of the smoothing parameter ε because of the very strong damping of the contributions of orbits with large lengths due to the exponential factor in eq.(179). This in principle gives the possibility to determine the semiclassical energies with an arbitrary accuracy. For that reason the Gaussian smoothing can be considered as an alternative to an analytical continuation of the periodic-orbit sum for the trace of the Green function $g(E)$, in case this sum is not convergent.

Again a relation between the momentum resolution, which is attainable with a finite number of orbits and the smoothing parameter ε is obtained by requiring that the momentum resolution is not decreased by smoothing the trace formula. The requirement that between two peaks that are separated by Δp the smoothed level density falls off to half of the value, that it has at the peaks, leads to the following condition ($p \gg \Delta p$)

$$1 + \exp\{-\frac{(\Delta p)^2}{\varepsilon^2}\} = 4 \exp\{-\frac{(\Delta p)^2}{4\varepsilon^2}\} \ , \tag{180}$$

which yields approximately

$$\varepsilon = \Delta p / 2.35 \ . \tag{181}$$

A comparison with eq.(177) shows that this value of ε is about 2/3 of the corresponding value of the smoothing parameter α of the Breit-Wigner smoothing.

In figure 22 the Gaussian smoothed level density is shown for $\varepsilon = 0.1$. The full line is the result of the periodic-orbit theory and the dashed curve is obtained from the quantum mechanical energy spectrum. The results are similar to the results of figure 20. Most of the remarks that have been made in connection with the Breit-Wigner smoothing can also be made here. But in details there are some differences. Between two peaks that are separated by a momentum difference, which is larger than the momentum resolution Δp, the Gaussian smoothed level density falls off to a smaller minimum value than the Breit-Wigner smoothed level density. This means that the Gaussian peaks are more distinct than the Breit-Wigner peaks. In addition the background from close neighbouring peaks is in case of the Gaussian smoothing smaller than in case of the Breit-Wigner smoothing because of the stronger falling off of a Gaussian peak. A further difference is that the agreement between the height of the dashed peaks and the full peaks is in the Gaussian case in general better than in case of the Breit-Wigner smoothing, because the contributions of long orbits, that are neglected in the sum over periodic orbits, are more suppressed. For these reasons the Gaussian smoothing is preferable over the Breit-Wigner smoothing.

In figures 23 a) and c) the results of an evaluation of the trace formula are shown for the energy range $0 < E < 1500$. Figures 23 b) and d) show a section of a) and c), respectively, and compare it to the corresponding curves, which are obtained from the energy spectrum. The

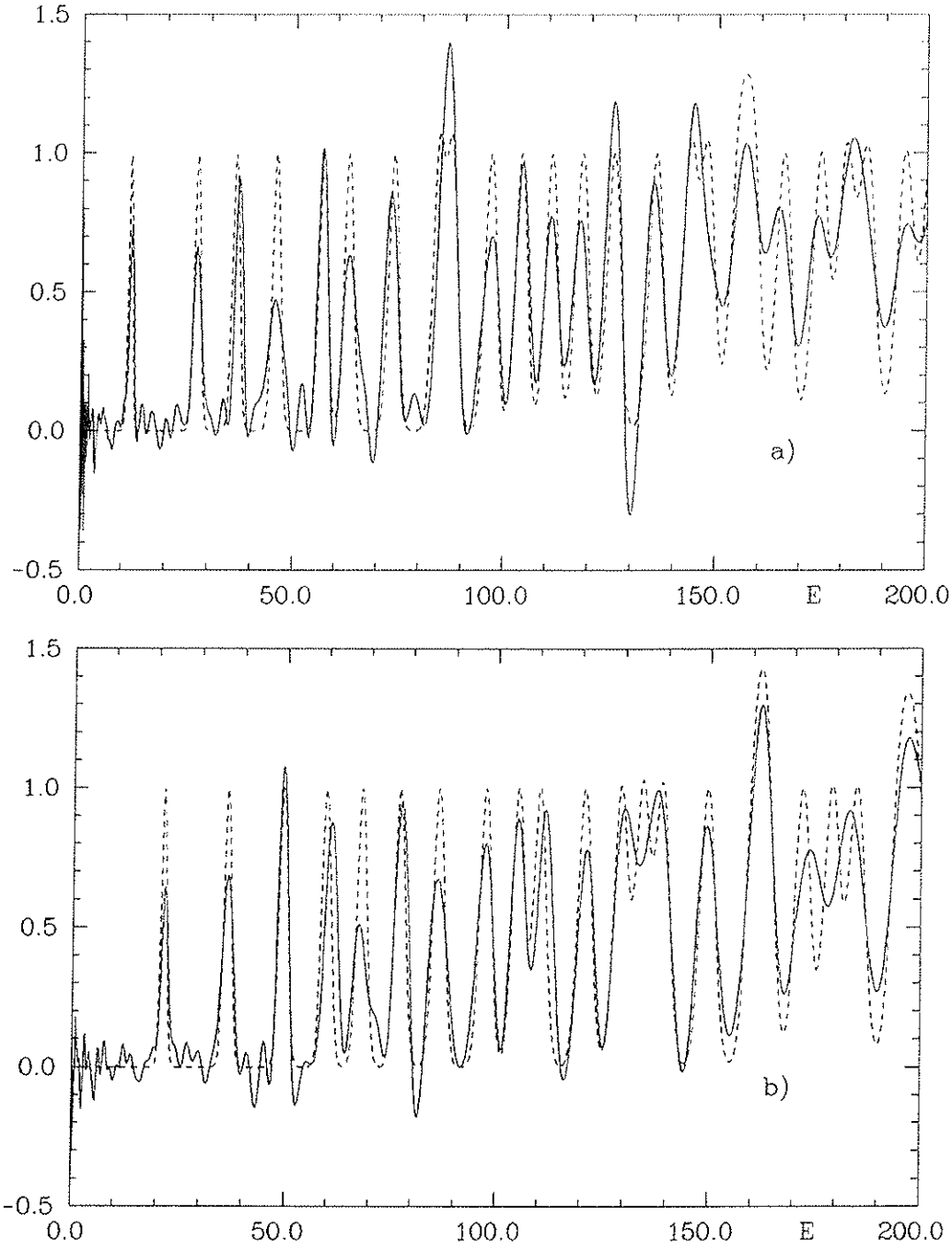

Figure 22: The Gaussian smoothed level density calculated from the periodic-orbit theory (full line) and the quantum mechanical energy spectrum (dashed line) for the energy eigenvalues of a) even and b) odd wavefunctions. The smoothing parameter is equal to $\varepsilon = 0.1$.

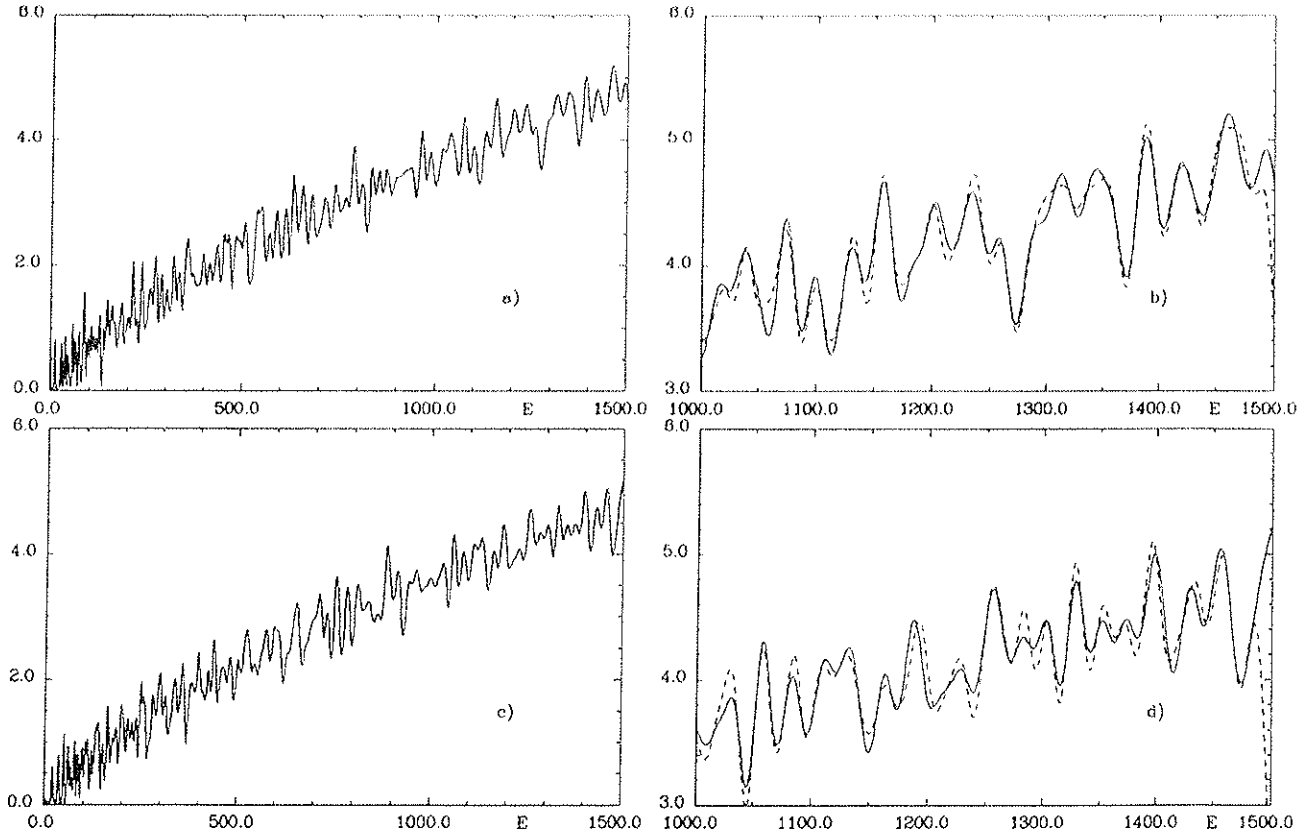

Figure 23: The periodic-orbit approximation for the Gaussian smoothed level density with $\varepsilon = 0.15$ for the eigenvalues of a) even and c) odd wavefunctions. b) and d) show a section of a) and c), respectively, in comparison with corresponding curves, that are obtained from the quantum mechanical energy spectrum (dashed line).

smoothing parameter is $\varepsilon = 0.15$. Again there is a good agreement between the corresponding curves. In comparison with figures 21 b) and d) the peaks are more marked and the fall off of the dashed curves close to $E = 1500$ occurs later, which is expected because of the stronger falling off of a Gaussian peak.

V.5 The Sine^3-Smoothed Energy Density

It is possible to choose the smoothing function $h(p')$ in such a way that its Fourier cosine transform is zero above a certain value of its argument. As a consequence the periodic-orbit sum is a sum over a finite number of orbits and can be done exactly. This gives the opportunity to examine the accuracy of the periodic-orbit theory as approximative theory. One smoothing function, which has this property, is given by

$$h(p') = \frac{\sin^3[\frac{L}{3}(p-p')]}{[\frac{L}{3}(p-p')]^3} + \frac{\sin^3[\frac{L}{3}(p+p')]}{[\frac{L}{3}(p+p')]^3} \quad , \tag{182}$$

with the Fourier cosine transform

$$g(x) = \frac{27}{8L^3}\cos(px)\begin{cases} 2(L^2/3 - x^2) & , \quad x < L/3 \\ (L-x)^2 & , \quad L/3 < x < L \\ 0 & , \quad L < x \end{cases} . \tag{183}$$

Figures 24 a) and b) show a plot of the $\sin^3$-smoothed level density for the eigenvalues of even and odd wavefunctions, respectively. The cut-off length is chosen to be $L = 20$, since all orbits with length below $L = 20$ are known. In this figure the effect of the semiclassical approximation can be seen directly. The main features of the dashed curves, which are obtained from the energy spectrum, are reproduced by the full curves, which are the result of the periodic-orbit theory. But in details there are deviations. The main difference between the full curves and the dashed curves is the height of the peaks. Most of the peaks of the full curves are smaller than the corresponding peaks of the dashed curves, some are higher. The positions of the maxima of the peaks are only slightly shifted. This means that the approximations for the quantum mechanical energies do not differ much from the actual energies. The positions of the maxima of the peaks are given in tables 8 and 10. These values agree with the approximations for the energies only in case of isolated peaks. If neighbouring peaks are close together, the superposition of the peaks also shifts their maxima. For that reason only the first few energies can be read off. The accuracy is on an average 3 % of the mean level separation.

The energy resolution in figure 24 is distinctly smaller than in previous figures. This is the disadvantage of the exact evaluation of the periodic orbit- sum. Again a relation between the resolvable momentum difference Δp and the smoothing parameter L is obtained by requiring that between two peaks, which are separated by Δp, the level density falls off to half of the value that it has at the peaks. This yields the following condition ($p \gg \Delta p$)

$$1 + \frac{\sin^3(L\Delta p/3)}{(L\Delta p/3)^3} = 4\frac{\sin^3(L\Delta p/6)}{(L\Delta p/6)^3} , \tag{184}$$

which results in

$$\Delta p \approx 9.522/L . \tag{185}$$

For $L = 20$ this gives $\Delta p \approx 0.476$, which is about twice the value, that was obtained in previous cases.

V.6 The Trace of the Cosine-Modulated Heatkernel

Up to this point it was only considered how the classical periodic orbits determine the quantum mechanical energy spectrum. However, one can also ask the opposite question, what information about the classical orbits is contained in the energy eigenvalues of the Schrödinger equation. This point is examined by choosing an appropriate smoothing function $h(p')$, whose Fourier cosine transform has peaks at the lengths of the periodic orbits:

$$h(p') = \cos(p'L)\exp(-p'^2 t) , \tag{186}$$

$$g(x) = \frac{1}{4\sqrt{\pi t}}\left[\exp\{-\frac{(x-L)^2}{4t}\} + \exp\{-\frac{(x+L)^2}{4t}\}\right] . \tag{187}$$

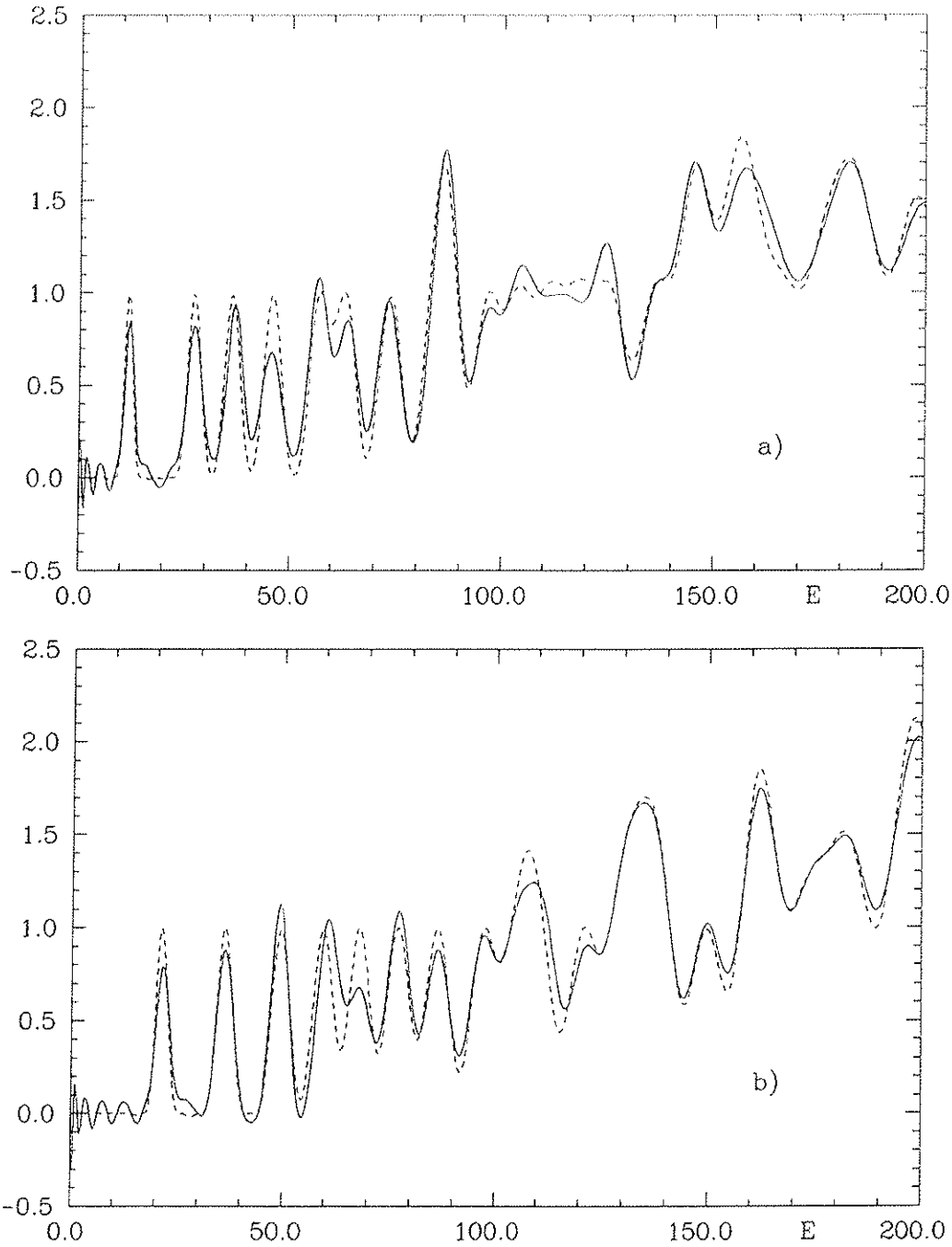

Figure 24: The sine^3-smoothed level density calculated from the periodic-orbit theory (full line) and the quantum mechanical energy spectrum (dashed line) for the energy eigenvalues of a) even and b) odd wavefunctions. The cut-off length is equal to $L = 20$.

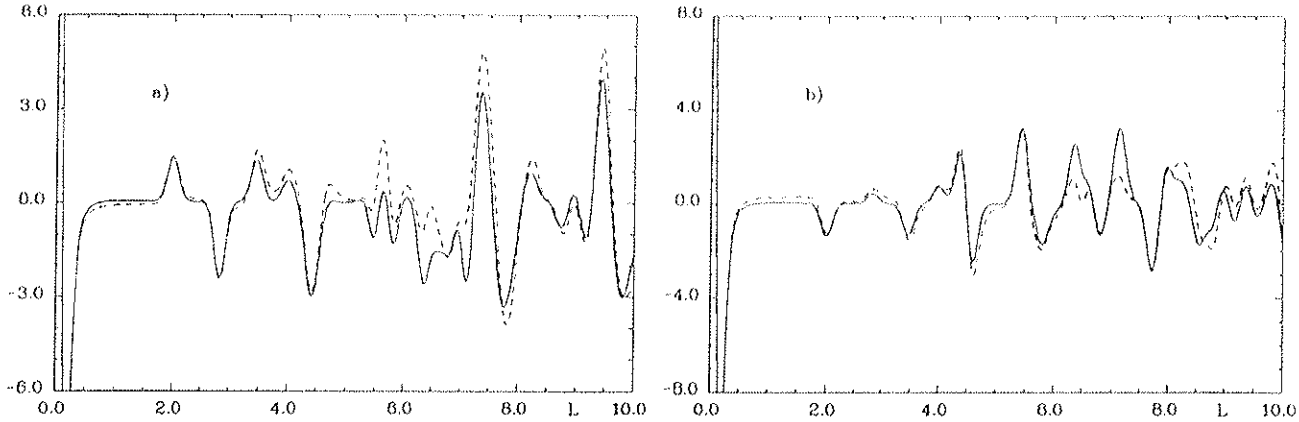

Figure 25: The trace of the cosine-modulated heat kernel with $t = 0.005$ calculated from the periodic-orbit sum (full line) and the quantum mechanical energy spectrum (dashed line) in case of a) even and b) odd symmetry.

The function $\sum_n h(p_n)$ is called the trace of the cosine-modulated heat kernel, since for $L = 0$ the trace of the heat kernel is obtained. The peaks at the lengths are positive or negative depending on the sign factor χ_γ^k in eq. (163). In figure 25 the cosine-modulated heat kernel is plotted with $t = 0.005$ for both symmetries. Only the first few peaks correspond to single lengths. The mean distance between neighbouring lengths is decreasing rapidly with increasing length, and for that reason the peaks above $L \approx 4.5$ in figure 25 are the superposition of several peaks at different lengths. The lengths of the ten shortest primitive periodic orbits are given in table 7. The second shortest orbit is the orbit along the line $y = x$ and in this case in table 7 the sign of its contribution to the periodic-orbit sum is given. There are also peaks at multiple repetitions of primitive orbits. For example the peak of a two times repetition of the shortest orbit can be seen in figures 25 a) and b) at $L = 4$.

	1	2	3	4	5	6	7	8	9	10
l_γ	2.000	2.828	3.464	4.395	4.559	4.596	5.414	5.474	5.547	5.796
a)	+1	+1	+1	−1	−1	+1	+1	−1	+1	−1
b)	−1	−1	−1	+1	−1	−1	+1	+1	−1	−1

Table 7: The lengths l_γ of the first ten periodic orbits of the desymmetrized hyperbola billiard and the sign factors χ_γ for a) even and b) odd symmetry.

V.7 The Dynamical Zeta Function

This section contains an evaluation of the representation of the dynamical zeta function by a sum over pseudo-orbits, which was derived in section II.4. Here we redefine the zeta function in terms of a new variable $s := -ip = -i\sqrt{E}$ by the equation $Z_{new}(s) = Z_{old}(E)$, because for billiard systems the sum over pseudo-orbits takes the form of a general Dirichlet series, if it

is expressed in terms of s. From equations (67) and (68) one then obtains

$$Z(s) = 1 + \sum_{n=1}^{\infty} A_n \exp(-sL_n) \quad , \tag{188}$$

where the sum extends over all pseudo-orbits of the system. The lengths L_n of the pseudo-orbits are obtained by all possible linear combinations of the lengths of all primitive periodic orbits

$$L_n = \sum_{i=1}^{k} m_i l_{\gamma_i} \quad , \tag{189}$$

where $k \geq 1$, m_i, $i = 1, \ldots, k$ are positive integers, and all γ_i are different. Again $Z^+(s)$ denotes the zeta function of the desymmetrized system with Neumann boundary conditions along the line $y = x$, and $Z^-(s)$ the zeta function of the system with Dirichlet boundary conditions along $y = x$. From equations (69), (65) and (66) one obtains

$$A_n = \prod_{i=1}^{k} \frac{(-1)^{m_i}(-1)^{m_i \tilde{n}_{\gamma_i}}(-1)^{n_{\gamma_i} m_i (m_i-1)/2} \exp\{-u_{\gamma_i} m_i (m_i-1)/4\}}{\prod_{j=1}^{m_i} |(\exp(u_{\gamma_i} j/2) - (-1)^{n_{\gamma_i} j} \exp(-u_{\gamma_i} j/2)| c_{\gamma_i,j}^{-1}} \quad , \tag{190}$$

where one has for $Z^+(s)$

$$c_{\gamma,j} = \begin{cases} -\exp(u_\gamma)[1 + (-1)^j \exp(j u_\gamma)]^{-1} & \text{for the orbit with code word } a = (\mathrm{b}) \\ 1 & \text{otherwise} \quad , \end{cases} \tag{191}$$

and for $Z^-(s)$

$$c_{\gamma,j} = \begin{cases} [1 + (-1)^j \exp(j u_\gamma)]^{-1} & \text{for the orbit with code word } a = (\mathrm{b}) \\ 1 & \text{otherwise} \quad . \end{cases} \tag{192}$$

In eq. (188) it is assumed that all pseudo-orbits are ordered in ascending order of their lengths: $L_n \leq L_{n+1}$, for $n \geq 1$. $s = \sigma + it$ is the complex variable of the Dirichlet series. The zeros s_n of $Z(s)$ on the negative imaginary axis or possibly close to this axis give approximations to the quantum mechanical energies: $s_n \approx -i\sqrt{E_n}$. A prerequisite for the determination of these zeros by an evaluation of eq. (188) is the convergence Dirichlet series in the considered region.

The open domain of absolute convergence of the series is some half-plane $\sigma > \sigma_a$, where σ_a is said to be the abscissa of absolute convergence of the Dirichlet series. The half-plane of convergence is given by $\sigma > \sigma_c$, where σ_c is the abscissa of convergence; $\sigma_c \leq \sigma_a$.

If $\sigma_a > 0$ it is determined by

$$\sigma_a = \overline{\lim_{n\to\infty}} \frac{1}{L_n} \log \sum_{\nu=1}^{n} |A_\nu| \quad , \tag{193}$$

and if $\sigma_c > 0$ it is determined by

$$\sigma_c = \overline{\lim_{n\to\infty}} \frac{1}{L_n} \log \left| \sum_{\nu=1}^{n} A_\nu \right| \quad . \tag{194}$$

These two equations are used for a numerical examination of the convergence properties of the Dirichlet series in eq. (188). All pseudo-orbits with length below $L = 20$ can be determined

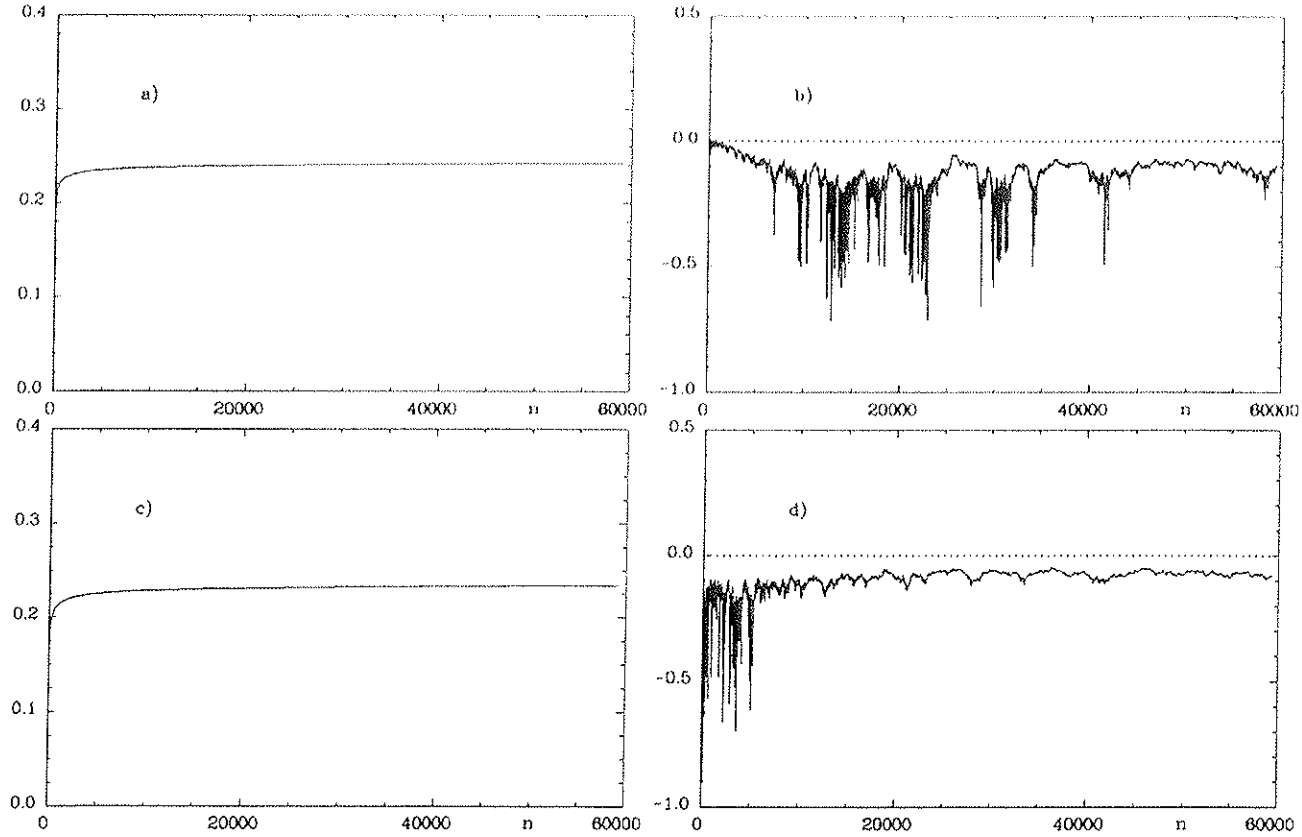

Figure 26: An evaluation of the sequences in equations (193) and (194), whose limit is the abscissa of a) absolute and b) conditional convergence of the Dirichlet series for the zeta function $Z^+(s)$. c) and d) show the corresponding evaluations for $Z^-(s)$.

completely, since all periodic orbits with length $l_i \leq 20$ are known. The combinations of the 13 098 periodic orbits with length below $l = 20$ give 59 370 pseudo-orbits with length below $L = 20$. Out of these pseudo-orbits 40 726 have different lengths.

Figure 26 shows an examination of the domains of absolute and conditional convergence of the Dirichlet series, which approximate the zeta functions $Z^+(s)$ and $Z^-(s)$, respectively. For both zeta functions figure 26 shows an evaluation of the two sequences, whose limiting value is considered in equations (193) and (194), in the range $1 \leq n \leq 59\,370$. In figures 26 a) and c) the absolute convergence is examined. The difference between both curves has its origin in the different contributions of the orbit along the straight line $y = x$ to the periodic-orbit sums, because all other orbits give identical contributions to the considered sequences in figures 26 a) and c). In case of the zeta function $Z^+(s)$, figure 26 a), the sequence approximates the value 0.242. Theoretically a value of 0.2415 is obtained from eq. (77), if the value of the topological entropy $\tau = 0.593$ is inserted, and if $\bar{\lambda}$ is set equal to the mean Lyapunov exponent 0.703. In figure 26 c) the limiting value is slightly smaller. It is equal to 0.234. The reason for this is that the contribution to $Z^-(s)$ of the orbit along $y = x$ is very small. This has a relatively large effect, since this orbit contributes to 11 007 pseudo-orbits. In figure 26 b) and d) the conditional convergence is examined. Both curves clearly are below zero. This suggests that the Dirichlet series for the two zeta functions possibly are convergent on the imaginary s-axis.

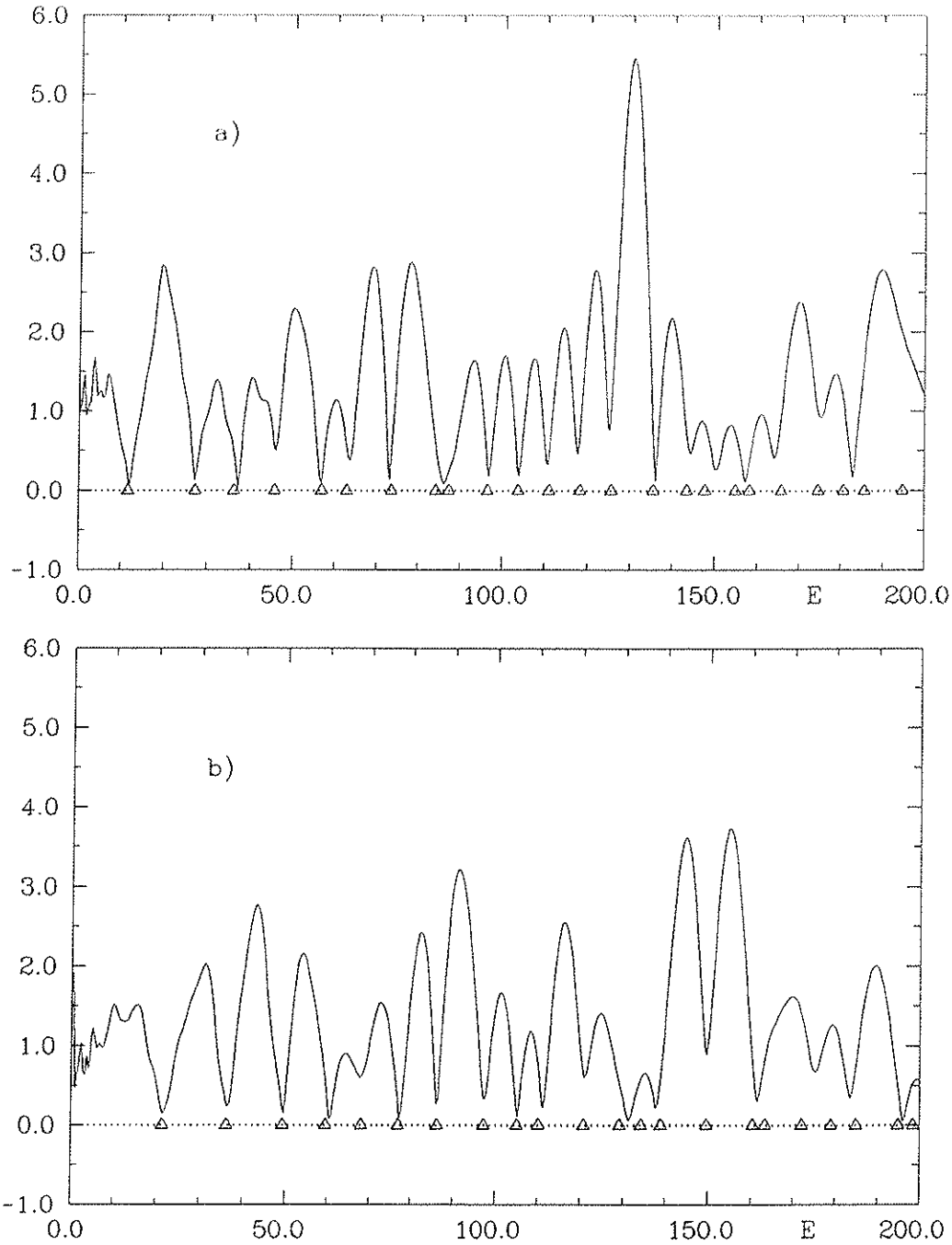

Figure 27: The absolute values of the zeta functions a) $Z^+(s)$ and b) $Z^-(s)$, $s = -i\sqrt{E}$. The triangles mark the positions of the energies.

In this case the zeros of $Z(s)$ can be computed from a convergent series.

Evaluation of the Dirichlet series are shown in figure 27. The sums are taken over all pseudo-orbits with length below $L = 20$. The figure shows a plot of the absolute values of $Z^+(s)$ and $Z^-(s)$, respectively, as functions of $E = -s^2$. The approximations to the zeta functions have no zeros on the imaginary s-axis in the range considered. But they have minima at positions, which are close approximations to the energy eigenvalues. For this reason the representation of the zeta functions by a sum over pseudo-orbits may be used as well as the previous periodic-orbit sums. The values of the energies, that are obtained, are listed in tables 8 and 10. The minimal momentum difference Δp, which can be resolved in figure 27, is estimated in the same way as it is for the unsmoothed level density, since the momentum dependence of a single term in the pseudo-orbit sum shows an analogous oscillatory behaviour. One obtains $\Delta p = 2\pi/20 \approx 0.314$.

V.8 The Riemann-Siegel Analogue

An approximation to the dynamical zeta function by a sum over a finite number of pseudo-orbits, whose number depends on the considered energy, was suggested by Berry and Keating [55]. This formula was proposed in analogy with the Riemann-Siegel formula for the Riemann zeta function $\zeta(z)$:

$$\zeta(z) = \sum_{n=1}^{\infty} \frac{1}{n^z} = \sum_{n=1}^{\infty} \exp(-z \log n) \quad . \tag{195}$$

This representation of $\zeta(z)$ by a Dirichlet series is convergent for $\mathrm{Re}\, z > 1$, and in the remaining complex z-plane $\zeta(z)$ is defined by analytic continuation. According to the Riemann hypothesis all the complex zeros of $\zeta(z)$ lie on the critical line $\mathrm{Re}\, z = 1/2$, where the Dirichlet series is divergent. The most effective computation of the zeros of $\zeta(z)$ is done by using the Riemann-Siegel formula, which is an asymptotic representation of $\zeta(z)$, that is valid on the critical line $\mathrm{Re}\, z = 1/2$. The dominant part of this formula is given by

$$\zeta(1/2 + iE) = 2\exp\{-i\pi\bar{\mathcal{N}}(E)\} \sum_{n=1}^{\mathrm{Int}[\sqrt{E/(2\pi)}]} \frac{\cos(\pi\bar{\mathcal{N}}(E) - E\log n)}{n^{1/2}} \quad . \tag{196}$$

Here the value of z on the critical line is denoted by $z = 1/2 + iE$. $\bar{\mathcal{N}}(E)$ is the mean approximation to the staircase function $\mathcal{N}(E)$, which is defined as the number of zeros z_n of the Riemann zeta function with imaginary part $0 < \mathrm{Im}\, z_n \leq E$. This notation is chosen because of an analogy between the zeros of $\zeta(z)$ and the quantum mechanical energy eigenvalues of a classically chaotic system, which is discussed in [50,16]. $\bar{\mathcal{N}}(E)$ is known analytically

$$\bar{\mathcal{N}}(E) = \frac{E}{2\pi}(\log\frac{E}{2\pi} - 1) + \frac{7}{8} \quad , \tag{197}$$

and the truncation condition for the series in eq. (196) is obtained by requiring, that the argument of the cosine is stationary with respect to the variable E.

Guided by the analogy between the Riemann zeta function and the dynamical zeta function $Z(s)$ of eq. (188), Berry and Keating conjectured a corresponding approximation for $Z(s)$ on the line $\mathrm{Re}\, s = 0$:

$$Z(-ip) \approx 2\exp\{i\pi\bar{N}(E)\} \sum_{n=1}^{n_{max}} A_n \cos(\pi\bar{N}(E) - pL_n) \quad , \tag{198}$$

where $E = p^2$, and $\bar{N}(E)$ is the mean approximation to the spectral staircase $N(E)$. The value n_{max} is determined by the condition $L_{n_{max}} \leq L_{max} < L_{n_{max}+1}$, and

$$L_{max} = 2\pi p \frac{\mathrm{d}}{\mathrm{d}E}\bar{N}(E) = 2\pi p\bar{d}(E) \quad , \tag{199}$$

where $\bar{d}(E)$ is the mean level density.

Formula eq. (198) has several advantages in comparison with previous applications of the periodic-orbit theory. The sum extends over a finite number of pseudo-orbits only, and the approximation for the combination $Z(-ip)\exp\{-i\pi\bar{N}(E)\}$ is real, so that the zeros of the right hand side of eq. (198) can be found by evaluating real functions only. The main disadvantage of formula (198) is the fact, that its derivation rests on analogy arguments and for that reason a numerical test of eq. (198) is of special importance.

The energy range over which the formula can be applied depends on the maximum length L_{max} in eq. (199) up to which all pseudo-orbits are known. With $L_{max} = 20$ and the generalized Weyl's law eq. (144), one obtains a maximal energy $E_{max} = 330.16$ for the approximation to $Z^+(s)$ and a value $E_{max} = 346.67$ for the approximation to $Z^-(s)$. In figures 28 and 29 an evaluation of the Riemann-Siegel lookalike formula of Berry and Keating is shown for the energy eigenvalues of even and odd wave functions up to the respective maximal energies. The actual energies are marked by triangles. The result of this evaluation is, that the formula gives quite good approximations to the energy eigenvalues. The approximations to the energies, which are determined from figures 28 and 29, are listed in tables 8-11 together with the actual energy values. In the case of the energy eigenvalues of even wavefunctions the mean absolute value of the deviation of the approximate energy values from the actual energy values is $\overline{\Delta E} = 0.46$. In comparison with the mean level spacing $1/\bar{d}(E)$ the deviation is on an average 6.5 %. The quotient of the deviation and the mean level spacing is varying much, but if it is averaged over several neighbouring energies, it is approximately constant. In case of the energy eigenvalues of odd wavefunctions the mean absolute value of the deviation of the approximate energies from the actual energies is $\overline{\Delta E} = 0.55$. The deviation is on an average 7.8 % of the mean level spacing. The quotient of the deviation and the mean level spacing also varies much, but its local average is slightly increasing with increasing energy, although this effect is not very significant.

The formula has some shortcomings. The approximation to $Z(-ip)$ is discontinuous. The maximum length L_{max} of pseudo-orbits which are included in the sum depends on the energy. If the energy is increased, then every time that L_{max} becomes equal to the length of a pseudo-orbit, the finite contribution of this pseudo-orbit is included in the sum, and this results in a discontinuity of the approximation of $Z(-ip)$. This leads especially to difficulties, if by such a discontinuity the functional value $Z(-ip) = 0$ is crossed. In the environment of some zeros of the curves in figures 28 and 29 the functions jump back and forth several times between positive and negative values, so that several zeros are close together. In those cases the values in tables 8-11 were determined by the average behaviour of the functions. More seriously, at some places where energy eigenvalues are, the curves miss to cross the zero-axis and thus give no approximations for these energies. This happens at the energies $E^+_{30} = 234.24$ and $E^+_{31} = 236.20$ of even wave functions, and at the energies $E^-_{37} = 296.38$ and $E^-_{38} = 298.05$ of odd wave functions. Although the curves have a maximum and a minimum, respectively, close to these energy values, these extrema do not extend beyond the zero-axis. A possibility to overcome this difficulty is to take the value of the position of the extremum

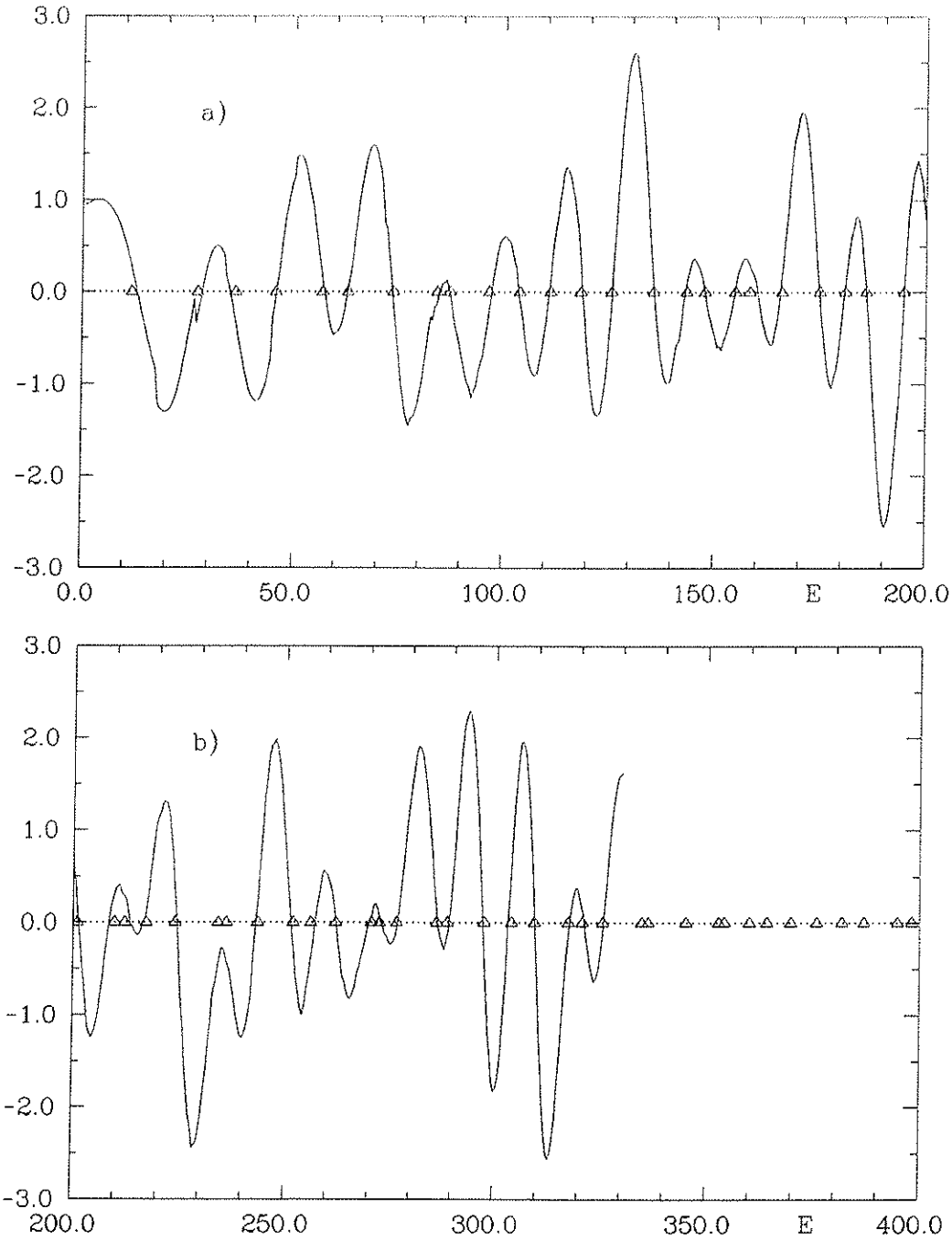

Figure 28: The evaluation of the Riemann-Siegel lookalike formula of Berry and Keating for the function $Z^+(s)\exp\{-i\pi\bar{N}^+(E)\}/2$, $s = -i\sqrt{E}$.

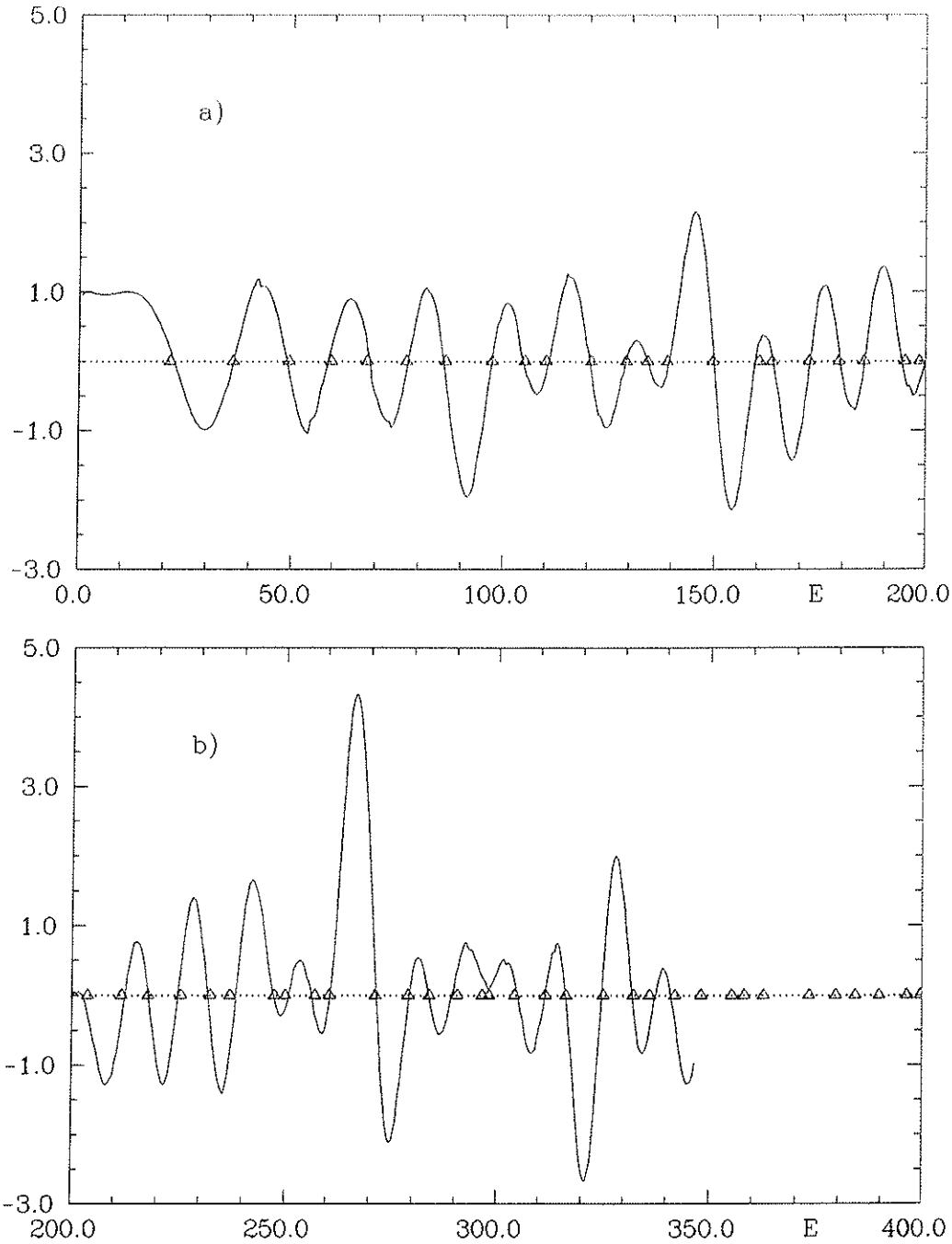

Figure 29: The evaluation of the Riemann-Siegel lookalike formula of Berry and Keating for the function $Z^{-}(s)\exp\{-i\pi\bar{N}^{-}(E)\}/2$, $s = -i\sqrt{E}$.

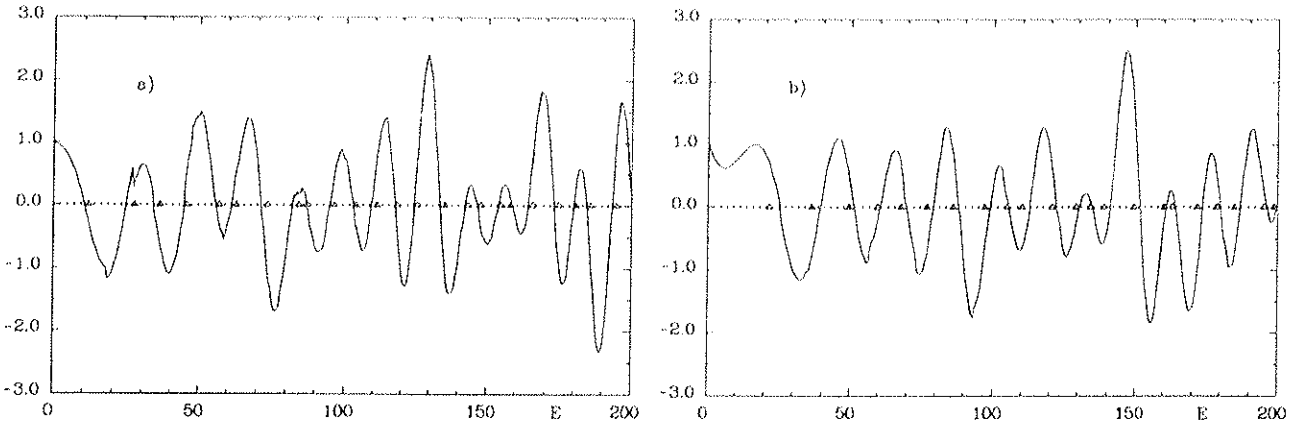

Figure 30: The same as in figures 28 and 29 for a) even and b) odd symmetry, evaluated with asymptotic laws for the mean staircase functions $\bar{N}^+(E)$ and $\bar{N}^-(E)$, which do not contain a constant term.

as approximation for the respective two energy values, but in more complicated cases this method might not be applicable in a unique way.

For the evaluation of formula(198) it is of utmost importance to use a very accurate formula for the mean spectral staircase $\bar{N}(E)$. For the computation of figures 28 and 29 also the constant corrections to $\bar{N}^+(E)$ and $\bar{N}^-(E)$, which were determined numerically from figure 12, were included in the formula for mean spectral staircases. If those constant corrections are neglected, the approximate energies show a clear shift. For a demonstration of this effect the results of the evaluation of eq. (198) with a generalized Weyl's law for $\bar{N}^+(E)$ and $\bar{N}^-(E)$, respectively, without a constant term is shown in figure 30. Here the agreement between approximate energies and actual energies is clearly not as good as in figures 28 and 29. In case of the energies of even wave functions the energy values are shifted on an average by $\Delta E = 1.32$ in direction to lower energies in comparison with the results of figure 28. The maximal shift is $\Delta E = 3.94$. In the case of the energies of odd wave functions the shift is on an average $\Delta E = 1.47$ in direction to higher energies, and the maximal shift is $\Delta E = 2.88$.

One of the main advantages of the formula (198) is the fact that a distinctly larger number of energies can be determined in comparison with previous methods. In case of the unsmoothed level density the resolution of two energies, which are separated by the mean level distance $1/\bar{d}(E)$ at energy E, requires the summation over all orbits with length up to

$$l \approx \frac{2\pi}{\Delta p} \approx \frac{4\pi p}{\Delta E} = 4\pi p \bar{d}(E) \quad . \tag{200}$$

This is exactly twice the value, which is given in eq. (199). Because of the exponential proliferation of the number of periodic orbits this means that the determination of a comparable number of energies requires in case of the Riemann-Siegel lookalike formula roughly the square root of the number of orbits, which are needed for the application of the trace formula for the unsmoothed level density. In this argument it is assumed that the distances between neighbouring energy levels do not deviate much from the mean level distance. On the other hand the good numerical results for the application of formula (198) may also partially be due to the fact, that the spectrum of the desymmetrized hyperbola billiard is very rigid, and that

there are only few pairs of adjacent energy values, which are close together. The problem that at some eigenvalues the curves miss to cross the zero-axis may occur more often in case that short level spacings occur more frequently. Besides this fact formula(198) shares with the original trace formula the problem that in order to achieve the resolution of the mean momentum difference $\overline{\Delta p}/2$ one needs the square of the number of orbits, which are required for the resolution of $\overline{\Delta p}$.

a)	b)	c)	d)	e)	f)	g)	h)
11.74	12.06	11.97	12.08	12.09	11.98	12.05	13.02
27.33	27.16	27.22	27.24	27.24	27.39	27.27	28.26
36.28	36.91	37.12	36.95	36.96	36.91	37.17	34.96
45.79	45.50	46.27	45.54	45.55	45.55	45.97	45.85
56.93	56.68	56.70	56.72	56.72	56.73	56.64	57.29
62.90	62.93	62.94	63.02	63.01	63.49	63.53	62.66
73.62	73.08	73.17	73.01	72.97	73.10	73.09	73.40
84.21 87.34	86.23	85.97	86.28	86.27	86.28	86.05	84.71 86.97
96.55	97.18	96.73	96.91	96.79	96.96	96.81	97.07
103.83	104.05	104.03	104.09	104.07	104.63	103.93	103.42
111.10 118.29	110.94 117.81	111.08 118.06	110.95 117.82	110.96 117.80	113.97	110.61 117.63	110.67 118.54
125.63	125.59	125.68	125.49	125.51	124.42	125.02	125.67
135.55	134.60	134.50	134.97	134.93		135.97	135.54
143.36 147.66	143.97 149.03	144.39	144.24	144.25	145.22	144.17 150.24	142.94 147.50
154.84 158.17	155.78	156.11	156.54	156.52	157.48	157.14	154.67 160.02
165.76	164.45	164.50	164.34	164.51		164.07	165.24
174.64	173.54	174.23	173.97	173.99		175.17	174.48
180.73 185.77	182.43	183.19	182.44	182.50	181.86	182.87	180.52 185.73
194.85	194.44	193.93	195.30	195.28	199.73		194.85

Table 8: The energy eigenvalues of even wavefunctions in comparison with values that are obtained from various applications of periodic-orbit sums. The different rows contain: a) the energy eigenvalues; the positions of the maxima of b) the unsmoothed energy density, c) the unsmoothed energy density using orbits with lengths below $l = 20$ only, d) the Breit-Wigner smoothed energy density with $\alpha = 0.15$, e) the Gaussian smoothed energy density with $\varepsilon = 0.1$, f) the sine^3-smoothed energy density with $L = 20$; g) the positions of the minima of the zeta function; h) the positions of the zeros of the Riemann-Siegel analogue.

a)	h)	a)	h)	a)	h)	a)	h)
200.98	201.22	236.20	—	272.40	272.84	309.37	309.41
209.82	208.45	243.51	243.07	276.50	276.74	317.45	317.67
212.22	213.42	251.90	251.37	286.15	286.44	320.78	321.15
217.22	216.83	256.03	257.03	288.73	289.16	325.64	325.72
224.12	224.56	262.00	261.95	297.49	297.13		
234.24	—	270.44	269.70	303.97	303.12		

Table 9: The same as in table 8 for energies above $E = 200$ for the rows a) and h) only.

a)	b)	c)	d)	e)	f)	g)	h)
21.46	21.72	21.82	21.74	21.74	21.75	21.54	22.33
36.28	36.30	36.33	36.38	36.40	36.29	36.54	36.41
49.43	49.26	49.48	49.31	49.32	49.23	49.55	48.87
59.50	60.76	60.47	60.75	60.71	60.75	60.57	58.71
67.94	67.22	67.05	67.30	67.31	67.83	67.67	68.75
77.04	77.51	77.67	77.47	77.47	77.18	77.36	77.38
86.24	85.71	85.39	85.96	85.93	86.33	86.16	85.72
97.27	97.40	97.15	97.32	97.25	97.27	97.40	97.10
105.12	104.98	104.78	105.05	105.00	108.90	105.20	104.76
110.21	111.50	111.94	111.45	111.51		111.24	110.86
120.81	121.42	120.74	121.33	121.24	121.86	120.99	120.43
129.20	129.36	130.06	130.13	130.03	134.66	131.37	129.03
134.24	138.02	138.14	137.51	137.65		137.77	134.46
138.86							139.23
149.54	149.15	149.23	149.30	149.29	149.68	149.49	149.71
160.39	162.24	161.88	162.13	162.06	162.11	161.45	159.33
163.34							163.59
172.02	173.96	173.17	174.00	173.76	181.88	175.22	172.16
179.04	183.13	183.59	183.16	183.25		183.57	179.31
185.01							185.08
194.91	196.74	196.48	197.29	197.11	199.19	196.14	194.00
198.47							200.14

Table 10: The energy eigenvalues of odd wavefunctions in comparison with values that are obtained from various applications of periodic-orbit sums. The different rows contain: a) the energy eigenvalues; the positions of the maxima of b) the unsmoothed energy density, c) the unsmoothed energy density using orbits with lengths below $l = 20$ only, d) the Breit-Wigner smoothed energy density with $\alpha = 0.15$, e) the Gaussian smoothed energy density with $\varepsilon = 0.1$, f) the $\sin^3$-smoothed energy density with $L = 20$; g) the positions of the minima of the zeta function; h) the positions of the zeros of the Riemann-Siegel analogue.

a)	h)	a)	h)	a)	h)	a)	h)
203.72	202.34	247.42	247.18	283.85	283.69	316.33	316.23
211.62	212.42	250.03	250.86	290.43	289.23	325.16	324.67
217.87	217.94	257.12	256.31	296.38	—	332.28	331.91
225.55	224.82	260.54	260.59	298.05	—	336.03	337.26
232.43	231.81	271.25	271.46	304.13	304.93	341.91	340.96
237.04	238.42	278.91	279.08	311.47	311.37		

Table 11: The same as in table 10 for energies above $E = 200$ for the rows a) and h) only.

VI Summary

The content of this paper can be divided into two parts. One part contains a detailed numerical examination of classical and quantum mechanical properties of a strongly chaotic system. This system is the so-called hyperbola billiard, a system which has several specific properties, which facilitate such a numerical investigation in comparison with other chaotic systems. There is a very efficient code that allows the classification of all periodic orbits by combinations of three different letters. In addition an extremum principle can be formulated for the periodic orbits, which makes a very fast and very accurate determination of the periodic orbits possible. This method avoids the problem of the exponential divergence of neighbouring trajectories, which is a specific property of chaotic systems. On the quantum mechanical side the first 578 energy levels of the hyperbola billiard were determined by a boundary element method, which for this system turned out to be much more efficient than other methods.

The examination of the classical and quantum mechanics of the hyperbola billiard can be considered as an independent investigation of certain properties of a chaotic system. However, the quantities which have been examined were partly selected in view of an investigation of the periodic-orbit theory of Gutzwiller. A detailed examination of the properties of this theory on the example of a strongly chaotic system is the second main part of this paper. The periodic-orbit theory supplies semiclassical approximations to quantum mechanical energies of classically chaotic systems by a sum over classical periodic orbits. For that reason it can be considered as a substitute for the EBK quantization rules, which can be applied to integrable systems only. The structure of the trace formula of the periodic-orbit theory is, however, much more complicated than the structure of the EBK quantization conditions. Due to this fact only very little is known about general analytical properties of the trace formula, although there have been many publications concerning the periodic-orbit theory in recent years. For a deeper understanding and an effective application of the periodic-orbit theory questions like the following remain to be answered:

— What are the properties and what is the quality of the semiclassical approximations for the quantum mechanical energies?

— What are the convergence properties of the periodic-orbit sums?

— How can the information about the energies be extracted most efficiently from the periodic orbits?

The intention of this work is to examine these questions numerically on the example of one special system, which allows relatively extensive investigations with the use of a reasonable amount of computer time. In detail the content of this work is the following:

After an introduction in chapter I, parts of the derivation of the periodic-orbit theory are discussed in chapter II. Special emphasis is given to the treatment of systems with discrete geometrical symmetries. For these systems the effectiveness of the periodic-orbit theory is increased by applying it to desymmetrized subsystems of the original system. An alternative formulation of the periodic-orbit theory is given in terms of a dynamical zeta function. This zeta function is defined by an infinite product over all periodic orbits, or by a series over all combinations of periodic orbits, which are denoted by pseudo-orbits. The convergence properties of the Gutzwiller trace formula are discussed. In general the periodic-orbit sum is

not convergent for real values of the energy E and thus a direct evaluation of the trace formula on the real energy-axis is not possible. A solution to this problem consists in a smoothing of the original trace formula. It is shown on the example of strongly chaotic billiard systems how smoothed trace formulae can be obtained in a mathematically correct way. These trace formulae contain absolutely convergent series and integrals only and in principle allow the determination of all semiclassical energies.

Properties of the classical periodic orbits of the hyperbola billiard are discussed in chapter III. The code for the orbits of the full hyperbola billiard is introduced. This code not only provides a unique classification of the periodic orbits. Also certain informations about the geometrical form and about symmetries of an orbit are contained in a code word. Vice versa symmetries impose restrictions on the form, code words can have. The general form of code words with a certain symmetry is given and formulae for their numbers are derived. For the desymmetrized hyperbola billiard the code is modified in order to provide a suitable description of the properties of the orbits of the desymmetrized system. All the orbits of the desymmetrized system with code words that consist of at most 14 letters were determined. The distributions of lengths and Lyapunov exponents of all orbits with a fixed code length N were examined, and it was found that these distributions show a significant behaviour, if N is large enough.

The lengths of the periodic orbits with a fixed value of N are to a good approximation Gaussian distributed, and the mean value of this distribution increases proportional to the code length N. The standard deviation increases like $\sqrt{N}$. This very regular behaviour allows an analytical examination of the behaviour of the number $\mathcal{N}(l)$ of orbits with length $l_\gamma \leq l$. On the assumption that the regular dependence on N of the length distributions holds also for $N > 14$ the leading term of the asymptotic behaviour of $\mathrm{d}\mathcal{N}(l)/\mathrm{d}l$ for large values of l is derived. The result is in full agreement with the expected asymptotic form for chaotic systems $\mathrm{d}\mathcal{N}(l)/\mathrm{d}l \sim \exp(\tau l)/l$, $l \to \infty$. A value of $\tau = 0.58$ is obtained for the topological entropy. The special properties of the distributions of lengths can be given a further interpretation. The Gaussian form of the distributions and the N-dependence of their mean values and their standard deviations agrees with the expectation for a one-dimensional random walk process consisting of N steps, where each step is carried out in average with a constant mean-free path and a constant standard deviation. This result already points to a possible random distribution of the lengths of the periodic orbits.

The Lyapunov exponents also are well approximated by Gaussian distributions, if the code length N is large enough. In this case the mean value of the distributions is approximately independent of N and the standard deviation decreases proportional to $1/\sqrt{N}$.

An accurate analysis of the properties of the trace formula requires the knowledge of all periodic orbits, whose length is below a certain value l. A complete determination of these orbits is possible in case of the hyperbola billiard due to certain correlations between orbit lengths and properties of the code words. All orbits with lengths $l_\gamma \leq 20$ were determined, which were 13 098 orbits altogether. With the input of these orbits the topological entropy τ was determined numerically with the result $\tau = 0.593$.

Finally the statistical properties of the total distribution of lengths were examined. This was possible since a sufficient part of the lower length spectrum is known completely. The statistical properties of the length spectrum were studied by means of the nearest neighbour spacings distribution, the scaled deviations of the lengths from their mean values, the number variance and the rigidity. Almost all the results are in agreement with a Poisson distribution.

Only for very long-range correlations the number variance shows a significant deviation from the Poisson distribution. This indicates that the lengths are in some sense randomly distributed with the restriction that very long-range correlations depend on specific properties of the considered system. The analogy with corresponding properties of the energy spectrum suggests a possible generalization of this result to other chaotic systems.

Chapter IV contains an examination of the energy spectrum of the hyperbola billiard, which is divided into partial energy spectra of even and odd eigenfunctions of the Hamiltonian operator, respectively. The boundary element method by which the energy eigenvalues of the Schrödinger equation are determined is discussed. The mean behaviour of the energy spectrum is described by the mean spectral staircase $\bar{N}(E)$. The first three leading terms of the asymptotic expansion of $\bar{N}(E)$ are known analytically. The correction to this approximation is examined numerically for both partial spectra of the hyperbola billiard. It is found that the correction terms are to a very good approximation constant for both spectra. The difference between the constants for the two partial spectra can also be determined analytically, and this value is in good agreement with the numerically obtained value. One of the most common tools for the examination, if quantum systems have a classical chaotic limit, is the consideration of the energy statistics. Short-range correlations in the energy spectrum are examined by considering the nearest neighbour spacings distribution $P(S)$. The results for this statistics are in agreement with the expectations for chaotic systems that are invariant under time reversal, that is with the GOE-statistics. The long-range correlations are investigated by considering the number variance $\Sigma^2(L)$ and spectral rigidity $\Delta_3(L)$. Here the results do not agree in all points with the expectations for generic chaotic systems. According to the semiclassical theory of Berry it is expected that for small values of the parameter L systems show universal behaviour, which in case of the hyperbola billiard corresponds to GOE-statistics. With increasing parameter L there will be a deviation from the universal behaviour, and for $L \to \infty$ both statistics saturate at a final value. Although the two partial spectra of the hyperbola billiard follow this general behaviour, the deviations from the GOE-curve occur at much smaller values of L than would be expected from Berry's theory. This disagreement between theory and numerical result can be explained by the fact that prerequisites of the theory are not satisfied in case of the hyperbola billiard. This is due to the infinite volume of the constant energy surface in phase space.

In chapter V the properties of several versions of periodic-orbit approximations are investigated numerically and the results are compared with each other. First the unsmoothed trace formula for the level density is considered. It is not known, if the periodic-orbit sum is convergent for real values of the energy E. For that reason the evaluation of the periodic-orbit sum is a numerical test, to what extend sensible results can be obtained from the trace formula. The sum was evaluated with all periodic orbits with code length $N \leq 14$ or length $l_\gamma \leq 20$, which are 533 760 orbits altogether. As result, all peaks at energy eigenvalues, which were expected to be resolved within the theoretically estimated energy resolution, were obtained from the trace formula. The approximations to the energy values are good down to the lowest energy despite of the semiclassical nature of the approximation. No clear indication of a divergence of the periodic-orbit sum was obtained. Thus the application of the unsmoothed trace formula yields good results in case of the hyperbola billiard. Notwithstanding no definite statement about the convergence of the sum can be obtained from this result. It is possible that although the series is divergent, nevertheless useful results can be obtained from the trace formula, if not too many orbits are included in the sum. Further

investigations of partial contributions to the periodic-orbit sum indicate, that the region of convergence at least reaches up very close to the axis of real momentum $p = \sqrt{E}$.

Two possibilities of smoothing the trace formula were considered next, the Breit-Wigner smoothing and the Gaussian smoothing. It was demonstrated, that even in case that an application of the unsmoothed trace formula gives good results, it is of advantage to smooth the trace formula slightly in order to improve the results. This improvement consists in an enhancement of single peaks and a suppression of background oscillations. Relations between suitable smoothing parameters and the maximal lengths of orbits that are included in the sum are given. The results for the Gaussian smoothing are slightly better than the results for the Breit-Wigner smoothing. The fact that the difference between both results is not bigger is due to the fact that for the considered system the application of the trace formula in its unsmoothed version already gives good results. In general the Gaussian smoothing can be used universally, while the applicability of the Breit-Wigner smoothing depends on the convergence properties of the unsmoothed periodic-orbit sum. The smoothed trace formulae were also evaluated in the range of higher energies, where no resolution of single energies can be achieved with the available number of periodic orbits. In this energy range, too, all the main features of the smoothed spectrum were reproduced by its periodic-orbit approximation.

A smoothing, which has the property, that the corresponding periodic-orbit sum is finite, is the so-called sine^3-smoothing. This smoothing has the advantage that both, the classical and the quantum mechanical side of the trace formula, can be evaluated with high accuracy, and both sides can thus be compared directly. This gives the possibility to see the effect of the semiclassical approximation. The result of the numerical evaluation is, that the classical and the quantum mechanical curves show a good agreement in their main features. Differences exist mainly in the heights of the peaks. The positions of the peaks are only slightly shifted. The disadvantage of evaluating the quantum mechanical side of the trace formula exactly is that one has to accept a lower energy resolution than in case of the unsmoothed trace formula.

An "inverse" application of the periodic-orbit theory, by which peaks at the lengths of periodic orbits are produced by a sum over quantum mechanical energies, is obtained by considering the periodic-orbit approximation for the trace of the cosine-modulated heat kernel. It is shown, that lengths of the periodic orbits can be determined from the energy spectrum.

Next the representation for the dynamical zeta function $Z(E)$ was examined. In case of billiard systems, this zeta function is expressed by a general Dirichlet series over all pseudo-orbits of the system. A numerical examination of convergence criteria for general Dirichlet series points to a convergence of the series for real values of the energy E. The pseudo-orbit representation of $Z(E)$ was evaluated numerically for both desymmetrized systems with all pseudo-orbits, which have a length below $L = 20$, which were 59 370 pseudo-orbits altogether. The absolute values of the obtained functions do not have zeros for real values of the energy E, but they show pronounced minima at positions, which are close to the energy eigenvalues. The energy resolution is about the same as in case of an application of the unsmoothed level density. The zeta function formalism thus can be used alternatively to the usual trace formula.

Finally the Riemann-Siegel lookalike formula of Berry and Keating was examined. This formula was proposed in analogy to the Riemann-Siegel formula for the Riemann zeta function and it approximates the zeta function $Z(E)$ by a finite but energy-dependent number of pseudo-orbits. This formula has the advantage that it can be evaluated exactly, and with

the input of the same number of pseudo-orbits a multiple of the number of energies can be obtained as in case of an evaluation of the semiclassical approximation for the level density. The numerical results were good. Altogether 87 approximations to energy eigenvalues were obtained. The accuracy is on an average about 7 per cent of the mean level spacing. The formula, however, also has some disadvantages. The approximation to $Z(E)$ is discontinuous. Some zeros are not unique in the sense that within a small energy interval the function jumps forth and back between positive and negative values several times, and for some energy values it does not give an approximation, since the curve misses to cross the zero-axis.

Summarizing the results for the periodic-orbit theory, the trace formula gives quite accurate approximations to the energy eigenvalues of the Schrödinger equation of a classically chaotic system. Within the limits of the numerical examinations no deviations from theoretical expectations have been discovered. More precisely, within the theoretically estimated energy resolution all expected peaks at energy eigenvalues or groups of energy eigenvalues were obtained. These results support the statement, that for chaotic systems the periodic-orbit theory can be considered as substitute for the EBK quantization rules. The main disadvantage of the periodic-orbit theory, which sets strong limits to its practical applicability, is the fact, that in going to higher energies the numerical effort for the resolution of single energies increases exponentially. For that reason it is very desirable to have powerful resummation techniques. The formula of Berry and Keating yields first good results. It is however important, to have a deeper understanding of this formula on a theoretical basis, since its derivation rests on analogy arguments. Furthermore, although this formula clearly increases the efficiency of the original trace formula, it shares the same problem of an exponentially increasing numerical effort for the resolution of higher energies.

Acknowledgements

I would like to thank Prof. F. Steiner for the kind supervision of my Ph. D. Thesis, for many fruitful discussions and for a lot of good advice. Furthermore I would like to thank R. Aurich for many valuable suggestions on tackling numerical problems. I also like to thank the Deutsche Forschungsgemeinschaft DFG for financial support.

Appendices

A Contributions of Orbits along the Boundary to the Zeta Function

In this appendix the form of the quantities $b_{\gamma,n}$ in equations (60) and (61), and of the quantities $c_{\gamma,j}$ in equations (65) and (66), is derived for periodic orbits, which run along the line $y = x$ only. More precisely, the contributions of these orbits to the periodic-orbit sum of a desymmetrized system is derived, whose corresponding full system is invariant under reflection on the line $y = x$.

The case of Neumann boundary conditions along the line $y = x$ is considered first. The starting point is the contribution of an orbit along $y = x$ to the oscillatory part of the trace of the Green function $g(E)$, which is given by equations (54) and (55). The transformations of this term are carried out analogously to the transformations in section II.4 for an ordinary orbit.

$$\begin{aligned}
& \frac{1}{i\hbar}\sum_{k=1}^{\infty}\frac{T_\gamma \exp\{ikS_\gamma(E)/\hbar - i\pi k\nu_\gamma/2\}}{\exp(ku_\gamma/2) - \sigma_\gamma^k \exp(-ku_\gamma/2)} \cdot \frac{1}{1+\sigma_\gamma^k\exp(-ku_\gamma)} \\
= & \frac{1}{i\hbar}\sum_{k=1}^{\infty}\frac{T_\gamma \exp\{ikS_\gamma(E)/\hbar - i\pi k\nu_\gamma/2\}}{\exp(ku_\gamma/2) - \exp(-3ku_\gamma/2)} \\
= & \frac{1}{i\hbar}\sum_{k=1}^{\infty}\frac{T_\gamma \exp\{ikS_\gamma(E)/\hbar - i\pi k\nu_\gamma/2 - ku_\gamma/2\}}{1-\exp(-2ku_\gamma)} \\
= & \frac{1}{i\hbar}\sum_{k=1}^{\infty}\sum_{n=0}^{\infty} T_\gamma \exp\{\frac{i}{\hbar}kS_\gamma(E) - \frac{i\pi}{2}k\nu_\gamma - \frac{ku_\gamma}{2} - 2knu_\gamma\} \\
= & \frac{1}{i\hbar}\sum_{n=0}^{\infty} T_\gamma \frac{\exp\{iS_\gamma(E)/\hbar - i\pi\nu_\gamma/2 - u_\gamma/2 - 2nu_\gamma\}}{1-\exp\{iS_\gamma(E)/\hbar - i\pi\nu_\gamma/2 - u_\gamma/2 - 2nu_\gamma\}} \\
= & \sum_{n=0}^{\infty}\frac{\mathrm{d}}{\mathrm{d}E}\log[1-\exp\{\frac{i}{\hbar}S_\gamma(E) - \frac{i\pi}{2}\nu_\gamma - u_\gamma(\frac{1}{2}+2n)\}] \quad . \qquad (201)
\end{aligned}$$

This result is compared with equations (57) and (59). The form of $b_{\gamma,n}$ in eq. (60) then follows directly. Eq. (201) is transformed further with the use of Euler's identity eq. (62):

$$\begin{aligned}
& \prod_{n=0}^{\infty}[1-\exp\{\frac{i}{\hbar}S_\gamma(E) - \frac{i\pi}{2}\nu_\gamma - u_\gamma(\frac{1}{2}+2n)\}] \\
= & \sum_{m=0}^{\infty}\frac{(-1)^m \exp\{imS_\gamma(E)/\hbar - i\pi m\nu_\gamma/2 - mu_\gamma/2 - u_\gamma m(m-1)\}}{\prod_{j=1}^{m}[1-\exp(-2ju_\gamma)]} \\
= & \sum_{m=0}^{\infty}\frac{(-1)^m \exp\{imS_\gamma(E)/\hbar - i\pi m\nu_\gamma/2 + u_\gamma(-m^2/2+m)\}}{\prod_{j=1}^{m}[\exp(ju_\gamma) - \exp(-ju_\gamma)]} \\
= & \sum_{m=0}^{\infty}\frac{(-1)^m \sigma_\gamma^{m(m-1)/2}\exp\{imS_\gamma(E)/\hbar - i\pi m\nu_\gamma/2 - u_\gamma m(m-1)/4\}}{\prod_{j=1}^{m}[\exp(ju_\gamma/2) - \sigma_\gamma^j\exp(-ju_\gamma/2)]} \\
& \times\prod_{j=1}^{m}\frac{\sigma_\gamma^{(j+1)}\exp(u_\gamma - ju_\gamma/2)}{\exp(ju_\gamma/2)+\sigma_\gamma^j\exp(-ju_\gamma/2)} \quad . \qquad (202)
\end{aligned}$$

The comparison with eq. (64) yields the form of $c_{\gamma,j}$ in eq. (65).

In the case of Dirichlet boundary conditions along the line $y = x$, the contribution of an orbit along $y = x$ to the oscillatory part of the trace of the Green function $g(E)$ is given by equations (54) and (56). The further steps are carried out as before

$$\begin{aligned}
& \frac{1}{ih}\sum_{k=1}^{\infty}\frac{T_\gamma \exp\{ikS_\gamma(E)/h - i\pi k\nu_\gamma/2\}}{\exp(ku_\gamma/2) - \sigma_\gamma^k \exp(-ku_\gamma/2)} \cdot \frac{1}{1+\sigma_\gamma^k\exp(ku_\gamma)} \\
= & \frac{1}{ih}\sum_{k=1}^{\infty}\frac{T_\gamma \exp\{ikS_\gamma(E)/h - i\pi k\nu_\gamma/2\}}{|\exp(3ku_\gamma/2) - \exp(-ku_\gamma/2)|\sigma_\gamma^k} \\
= & \frac{1}{ih}\sum_{k=1}^{\infty}\frac{T_\gamma \sigma_\gamma^k \exp\{ikS_\gamma(E)/h - i\pi k\nu_\gamma/2 - 3ku_\gamma/2\}}{1-\exp(-2ku_\gamma)} \\
= & \frac{1}{ih}\sum_{k=1}^{\infty}\sum_{n=0}^{\infty} T_\gamma \sigma_\gamma^k \exp\{\frac{i}{\hbar}kS_\gamma(E) - \frac{i\pi}{2}k\nu_\gamma - \frac{3}{2}ku_\gamma - 2knu_\gamma) \\
= & \frac{1}{ih}\sum_{n=0}^{\infty} T_\gamma \frac{\sigma_\gamma \exp\{iS_\gamma(E)/h - i\pi\nu_\gamma/2 - 3u_\gamma/2 - 2nu_\gamma\}}{1-\sigma_\gamma\exp\{iS_\gamma(E)/h - i\pi\nu_\gamma/2 - 3u_\gamma/2 - 2nu_\gamma\}} \\
= & \sum_{n=0}^{\infty}\frac{\mathrm{d}}{\mathrm{d}E}\log[1-\sigma_\gamma\exp\{\frac{i}{\hbar}S_\gamma(E) - \frac{i\pi}{2}\nu_\gamma - u_\gamma(\frac{3}{2}+2n)\}] \ . \qquad (203)
\end{aligned}$$

The comparison of this result with equations (57) and (59) gives the form of $b_{\gamma,n}$ in eq. (61). Euler's identity in eq. (62) is used again for the next steps

$$\begin{aligned}
& \prod_{n=0}^{\infty}[1-\sigma_\gamma\exp\{\frac{i}{\hbar}S_\gamma(E) - \frac{i\pi}{2}\nu_\gamma - u_\gamma(\frac{3}{2}+2n)\}] \\
= & \sum_{m=0}^{\infty}\frac{(-1)^m\sigma_\gamma^m\exp\{imS_\gamma(E)/\hbar - i\pi m\nu_\gamma/2 - 3mu_\gamma/2 - u_\gamma m(m-1)\}}{\prod_{j=1}^{m}[1-\exp(-2ju_\gamma)]} \\
= & \sum_{m=0}^{\infty}\frac{(-1)^m\sigma_\gamma^m\exp\{imS_\gamma(E)/\hbar - i\pi m\nu_\gamma/2 - m^2u_\gamma/2\}}{\prod_{j=1}^{m}[\exp(ju_\gamma) - \exp(-ju_\gamma)]} \\
= & \sum_{m=0}^{\infty}\frac{(-1)^m\sigma_\gamma^{m(m-1)/2}\exp\{imS_\gamma(E)/\hbar - i\pi m\nu_\gamma/2 - u_\gamma m(m-1)/4\}}{\prod_{j=1}^{m}[\exp(ju_\gamma/2) - \sigma_\gamma^j\exp(-ju_\gamma/2)]} \\
& \times\prod_{j=1}^{m}\frac{\sigma_\gamma^j\exp(-ju_\gamma/2)}{\exp(ju_\gamma/2)+\sigma_\gamma^j\exp(-ju_\gamma/2)} \ . \qquad (204)
\end{aligned}$$

The comparison with eq. (64) yields the result for $c_{\gamma,j}$ in eq. (66).

B Calculation of the Monodromy Matrix

Consider a certain periodic orbit. In its vicinity a coordinate system can be introduced, whose x-coordinate is parallel to the orbit, and whose y-coordinate is perpendicular to it. A particle that starts at $\vec{q} = (x_0, \mathrm{d}y)$ with momentum $\vec{p} = (p_x, \mathrm{d}p_y)$ infinitesimally close to the periodic trajectory will have after one traversal the coordinates $\vec{q}' = (x_0, \mathrm{d}y')$ and momentum $\vec{p}' = (p_x, \mathrm{d}p_y')$. The monodromy matrix M of the periodic orbit is then defined by

$$\begin{pmatrix} \mathrm{d}y' \\ \mathrm{d}p_y' \end{pmatrix} = M \begin{pmatrix} \mathrm{d}y \\ \mathrm{d}p_y \end{pmatrix} \quad . \tag{205}$$

It has the property $\det M = 1$. Introducing an angle α between momentum-direction and x-direction one obtains

$$\begin{pmatrix} \mathrm{d}y' \\ \mathrm{d}\alpha' \end{pmatrix} = \tilde{M} \begin{pmatrix} \mathrm{d}y \\ \mathrm{d}\alpha \end{pmatrix} \; , \; \tilde{M} = \begin{pmatrix} M_{11} & M_{12}p \\ M_{21}/p & M_{22} \end{pmatrix} \; , \; p = |\vec{p}| \; . \tag{206}$$

The matrix $\tilde{M}$ can be decomposed into partial matrices $\tilde{M}_i$

$$\tilde{M} = \tilde{M}_{i_{max}} \cdot \ldots \cdot \tilde{M}_2 \cdot \tilde{M}_1 \; . \tag{207}$$

This is done by traversing the periodic orbit once and inserting into the product one matrix $\tilde{M}_i$ for every straight line segment and for every reflection on the boundary. It follows from geometrical considerations that for a straight line segment the matrix $\tilde{M}_i$ is of the form

$$\tilde{M}_i = \begin{pmatrix} 1 & l_i \\ 0 & 1 \end{pmatrix} \; , \tag{208}$$

where l_i is the length of the line segment. For a reflection on the boundary the corresponding matrix $\tilde{M}_i$ has the form

$$\tilde{M}_i = \begin{pmatrix} -1 & 0 \\ 2(R_i \cos\beta_i)^{-1} & -1 \end{pmatrix} \; . \tag{209}$$

Here β_i is the angle between the incoming trajectory and the normal to the boundary. R_i is the radius of curvature of the boundary at the collision point. R_i is greater than zero if the boundary is convex and it is less than zero, if the boundary is concave. If the reflection takes place on a straight line, $R_i = \infty$.

In case that $|\mathrm{Tr}(M)| > 2$, the periodic orbit is unstable and M has eigenvalues $\Lambda_{1,2} = \exp(\pm u)$ or $\Lambda_{1,2} = -\exp(\pm u)$, where $u > 0$ is the stability exponent. The Lyapunov exponent λ of an unstable periodic orbit is defined as $\lambda = u/T$, where T is the period of the periodic orbit. If $|\mathrm{Tr}(M)| < 2$, the periodic orbit is stable and M has eigenvalues $\Lambda_{1,2} = \exp(\pm iv)$ where v is the angle of stability.

For billiards, whose boundaries consist of concave and straight pieces only, and which have the property that every classical trajectory is reflected from a concave part of the boundary at least once, it is easy to show that the product of matrices $\tilde{M} = \tilde{M}_{i_{max}} \cdot \ldots \cdot \tilde{M}_1$ satisfies the relation $|\mathrm{Tr}(\tilde{M})| > 2$. For that reason all periodic orbits of the hyperbola billiard are unstable and have positive stability exponents.

C Extremum Principle for Periodic Orbits

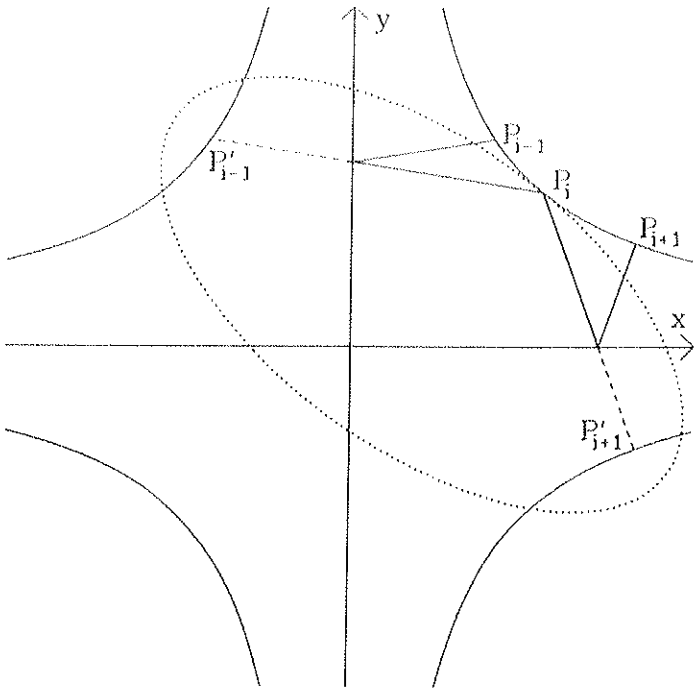

Figure 31: Illustration of the extremum principle

Suppose $P_{i-1}(x_{i-1}|1/x_{i-1})$, $P_i(x_i|1/x_i)$ and $P_{i+1}(x_{i+1}|1/x_{i+1})$ are three successive points of a periodic orbit on the hyperbola. The lengths of the segments of the periodic orbit from P_{i-1} to P_i and from P_i to P_{i+1} are denoted by $l_{i-1,i}$ and $l_{i,i+1}$, respectively. P'_{i-1} and P'_{i+1} are two points that are obtained by extending the two line segments of the orbit that have P_i as common point until they hit one of the hyperbolae $y = 1/x$ or $y = -1/x$ (see figure 31). Now consider an ellipse through P_i with foci P'_{i-1} and P'_{i+1}. Because of the focal property of the ellipse that the lines $P'_{i-1}P_i$ and $P'_{i+1}P_i$ form equal angles with the tangent to the ellipse at point P_i, it follows that the ellipse and the hyperbola have a common tangent at point P_i. It further holds that $l_{i-1,i} + l_{i,i+1} = A$, where A is the major axis of the ellipse. If now the position of the point P_i on the hyperbola is changed, one sees immediately that the major axis of the ellipse through P_i with foci P'_{i-1} and P'_{i+1} is increased and therefore also the sum of the distances $\overline{P'_{i-1}P_i}$ and $\overline{P_iP'_{i+1}}$. Since this argument holds for every point of the periodic orbit on the hyperbola, the following extremum principle for periodic orbits is obtained:

$$\frac{\partial}{\partial x_i} L(x_1, \ldots, x_N) = 0 \; \forall \, i = 1, \ldots, N \tag{210}$$

and

$$\frac{\partial^2}{\partial x_i^2} L(x_1, \ldots, x_N) > 0 \; \forall \, i = 1, \ldots, N \; , \tag{211}$$

where L is the length of a given periodic orbit as a function of its N points on the hyperbola, i.e.

$$L(x_1, \ldots, x_N) = \sum_{i=1}^{N} L_i(x_i, x_{i+1}) \; , \; x_{N+1} := x_1 \; . \tag{212}$$

There are three different possibilities for the functional dependence of the length $L_i(x_i, x_{i+1})$ of the segment of the orbit from $P_i(x_i|1/x_i)$ to $P_{i+1}(x_{i+1}|1/x_{i+1})$:

$$L_i(x_i, x_{i+1}) = \begin{cases} f_x(x_i, x_{i+1}) := |(x_i - x_{i+1})^2 + (1/x_i + 1/x_{i+1})^2|^{1/2} \\ f_y(x_i, x_{i+1}) := |(x_i + x_{i+1})^2 + (1/x_i - 1/x_{i+1})^2|^{1/2} \\ f_b(x_i, x_{i+1}) := |(x_i + x_{i+1})^2 + (1/x_i + 1/x_{i+1})^2|^{1/2} . \end{cases} \tag{213}$$

These three cases, respectively, correspond to segments in which there is a reflection on the x-axis only or on the y-axis only or on both axes. Thus if the given periodic orbit is represented by the ternary sequence $a = (a_1, \ldots, a_N)$, its length-function reads

$$L(x_1, \ldots, x_N) = \sum_{i=1}^{N} f_{a_i}(x_i, x_{i+1}) . \tag{214}$$

D Form and Number of Code Words with $\mathrm{R}a \equiv a$

In chapter III properties and numbers of code words, which have certain symmetries, are given. Since the derivations of these results are extensive, they are carried out here only for one symmetry, namely for code words with $\mathrm{R}a \equiv a$.

The following notation is used:

An orbit is considered, whose associated code word consists of N letters

$$a = (a_1, \ldots, a_N) \ . \tag{215}$$

This code word fixes the sense of direction, by which the orbit is traversed in coordinate space. The N points of the orbit, which lie on the hyperbola $y = 1/x$, are denoted by $P_1, \ldots, P_N$ in the sequence, in which they are met during one traversal of the orbit. Indices $i > N$ for the points P_i are allowed, with the condition that $P_{i+N} = P_i$.

From now on it is assumed, that the code word satisfies $\mathrm{R}a \equiv a$, and that the corresponding periodic orbit is invariant under reflection on the line $y = x$. Further it is assumed that this orbit is primitive. Consider an arbitrary point P_i of the N points of this orbit on the hyperbola. Then the point, which is obtained by reflecting the point P_i on the straight line $y = x$, also belongs to the set of points $\mathbf{P} = \{P_i | 1 \leq i \leq N\}$. Let this point be P_j. It is possible that several points of the set $\mathbf{P}$ satisfy this condition. Then the index j is determined by requiring, that the point P_{j+1} is obtained by reflecting the point P_{i+1} on the line $y = x$. Since the orbit is primitive, this uniquely fixes the index j. Now the orbit is traversed, starting at point P_i. During this traversal the point P_j is reached. Let $i + n = j \bmod N$, $n \leq N$. This means that the point P_j is reached after n reflections on the hyperbola. After n further reflections on the hyperbola one arrives at the starting point P_i again, because of the invariance of the orbit under reflection on the line $y = x$. Now two cases have to be distinguished. The first case is that $P_i = P_j$ and $i = j$. This is only possible if $N = 1$ and if the orbit runs along the line $y = x$ only. Such an orbit exists, and it corresponds to the code word $a = (\mathrm{b})$. The second case is that $i \neq j$. Then the length of the code word is even and it satisfies $N = 2n$. The code word must be of the form

$$a = c \oplus \mathrm{R}c \ , \tag{216}$$

where c is a word of length $N/2 - n$. This follows from the fact, that the part of the orbit from P_j to P_i is obtained by reflecting the part of the orbit from P_i to P_j along the line $y = x$. Eq. (216) is equal to eq. (93). Since the argument leading to eq. (216) does not depend on the choice of the starting point P_i, it further follows that every cyclic permutation of the word a must be of the general form of eq. (216).

Vice versa every code word, which is of the form of eq. (216), satisfies

$$\mathrm{R}a = \mathrm{R}(c \oplus \mathrm{R}c) = \mathrm{R}c \oplus c \equiv c \oplus \mathrm{R}c = a \quad , \tag{217}$$

that is, it belongs to an orbit, which is invariant under reflection on the line $y = x$. But it need not be a primitive periodic orbit. It can be a N-times repetition of the orbit with code word $a = (\mathrm{b})$ for example. If the underlying primitive code word is not equal to (b), then the number of repetitions must be odd, since if it is even and one traverses the periodic orbit, starting at point P_i, then after $n = N/2$ reflections on the hyperbola one arrives at the point $P_{i+n} = P_i$ and not at the point P_j, which is obtained by reflecting P_i on the line $y = x$. Taking this into consideration one obtains the following relation for the $3^{N/2}$ different code words a of the form in eq. (216):

$$3^{N/2} = \sum_{\substack{M|N \\ M\nmid(N/2)}} M \cdot Z_R(M) + Z_R(1) \quad , \tag{218}$$

where $Z_R(M)$ is the number of different primitive cyclic classes of code length M with the considered symmetry. $Z_R(M)$ is multiplied by M, since all M cyclic permutations of a primitive code word are different. With $Z_R(1) = 1$ eq. (94) is obtained.

References

[1] H. Poincaré, *Les Méthodes Nouvelles de la Mécanique Céleste*, Gauthier-Villars, Paris (1892).

[2] V. I. Arnold, *Mathematical Methods of Classical Mechanics*, Springer, New York (1978).

[3] J. L. Lebowitz and O. Penrose, Physics Today 26 (February 1973) 23.

[4] Ya. G. Sinai, Russ. Math. Surv. **25** (1970) 137.

[5] L. A. Bunimovich, Funct. Anal. Appl. **8** (1974) 254; Commun. Math. Phys. **65** (1979) 295.

[6] J. Hadamard, J. Math. Pure Appl. **4** (1898) 27.

[7] A. N. Kolmogorov, Dokl. Akad. Nauk. USSR **98** (1954) 527.

[8] V. I. Arnold, Russ. Math. Surv. **18** (1963) 5.

[9] J. Moser, Nachr. Akad. Wiss. Göttingen **1** (1962) 1.

[10] M. V. Berry, Lectures given at the Les Houches school on Chaos and Quantum Physics (August 1989), to be published by North-Holland.

[11] M. V. Berry, Proc. Roy. Soc. London **A 413** (1987) 183.

[12] O. Bohigas and M.-J. Giannoni, in *Mathematical and Computational Methods in Nuclear Physics*, edited by J. S. Dehesa, J. M. G. Gomez and A. Polls, Springer Lecture Notes in Physics No. 209 (1984) 1.

[13] A. Einstein, Verh. Dtsch. Phys. Ges. **19** (1917) 82.

[14] M. C. Gutzwiller, *Chaos in Classical and Quantum Mechanics*. Springer, New York (1990).

[15] M. V. Berry, Proc. Roy. Soc. London **A 400** (1985) 229.

[16] E. B. Bogomolny, preprint (1990), Comments At. Mol. Phys. in press.

[17] M. C. Gutzwiller, J. Math. Phys. **8** (1967) 1979, and **10** (1969) 1004, and **11** (1970) 1791, and **12** (1971) 343.

[18] C. Morette, Phys. Rev. **81** (1951) 848.

[19] G. J. Papadopoulos. Phys. Rev. **D 11** (1975) 2870.

[20] J. H. Van Vleck, Proc. Natl. Ac. Sc. USA **14** (1928) 178.

[21] J. W. Milnor, *Morse Theory*, Princeton University Press (1973).

[22] M. C. Gutzwiller, Lectures given at the Les Houches school on Chaos and Quantum Physics (August 1989), to be published by North-Holland.

[23] E. B. Bogomolny, Physica **D 31** (1988) 169.

[24] E. J. Heller, Phys. Rev. Lett. **53** (1984) 1515; in *Quantum Chaos and Statistical Nuclear Physics*, edited by T. H. Seligman and H. Nishioka, Springer Lecture Notes in Physics No. 263 (1986) 162.

[25] R. Aurich and F. Steiner, DESY preprint 90-018 (1990), Physica **D** (1991) in press.

[26] M. V. Berry, Proc. Roy. Soc. London **A 423** (1989) 219.

[27] M. Abramowitz and I. A. Stegun, *Handbook of Mathematical Functions*, National Bureau of Standards, Washington (1964).

[28] E. B. Bogomolny and E. J. Heller, preprint (1989).

[29] R. Balian and C. Bloch, Ann. Phys. (N.Y.) **69** (1972) 76, and **85** (1974) 514.

[30] M. V. Berry and M. Tabor, Proc. Roy. Soc. London **A 349** (1976) 101.

[31] M. V. Berry and M. Tabor, J. Phys. **A 10** (1977) 371.

[32] M. V. Berry, in *Chaotic Behaviour of Deterministic Systems*, Les Houches Lectures XXXVI, edited by G. Iooss, R. H. G. Helleman and R. Stora, North-Holland, Amsterdam (1983).

[33] M. V. Berry and K. E. Mount, Rep. Prog. Phys. **35** (1972) 315.

[34] B. Eckhardt, Phys. Rep. **163** (1988) 205.

[35] N. L. Balazs and A. Voros, Phys. Rep. **143** (1986) 109.

[36] R. Aurich, M. Sieber and F. Steiner, Phys. Rev. Lett. **61** (1988) 483; R. Aurich and F. Steiner, Physica **D 39** (1989) 169.

[37] R. Aurich and F. Steiner, Physica **D 32** (1988) 451; R. Aurich, E. B. Bogomolny and F. Steiner, Physica **D 48** (1991) 91.

[38] Results of the numerical work of C. Schmit are given in [35].

[39] R. Aurich and F. Steiner, Physica **D 43** (1990) 155.

[40] M. C. Gutzwiller, J. Math. Phys. **12** (1971) 343, and **14** (1973) 139, and **18** (1977) 806; Phys. Rev. Lett. **45** (1980) 150; Physica **D 5** (1982) 183; J. Phys. Chem. **92** (1988) 3154; Physica **D 38** (1989) 160.

[41] M. L. Du and J. B. Delos, Phys. Rev. Lett. **58** (1987) 1731.

[42] D. Wintgen and H. Friedrich, Phys. Rev. **A 36** (1987) 131.

[43] D. Wintgen, Phys. Rev. Lett. **58** (1987) 1589, and **61** (1988) 1803.

[44] M. Tabor, Physica **D 6** (1983) 195.

[45] J. P. Keating, Ph. D. Thesis, University of Bristol, U. K. (1989).

[46] M. V. Berry, Ann. Phys. (N.Y.) **131** (1981) 163.

[47] J. P. Keating and M. V. Berry, J. Phys. **A 20** (1987) L 1139.

[48] J. Bolte and F. Steiner, DESY preprint 90-082 (1990), submitted to Commun. Math. Phys..

[49] A. Voros, J. Phys. **A. 21** (1988) 685.

[50] M. V. Berry, in *Quantum Chaos and Statistical Nuclear Physics*, edited by T. H. Seligman and H. Nishioka, Springer Lecture Notes in Physics No. 263 (1986) 1.

[51] P. Cvitanović, Phys. Rev. Lett. **61** (1988) 2729.

[52] P. Cvitanović and B. Eckhardt, Phys. Rev. Lett. **63** (1989) 823.

[53] R. Artuso, E. Aurell and P. Cvitanović, Nonlinearity **3** (1990) 325 and 361.

[54] L. Euler, *Introductio in Analysin Infinitorum* (1748) §§ 306-307.

[55] M. V. Berry and J. P. Keating, J. Phys. **A 23** (1990) 4839.

[56] B. Eckhardt and E. Aurell, Europhys. Lett. **9** (1989) 509.

[57] M. Sieber and F. Steiner, Phys. Lett. **A 144** (1990) 159.

[58] M. Sieber and F. Steiner, Physica **D 44** (1990) 248.

[59] R. Aurich, Ph. D. Thesis, University of Hamburg (1990).

[60] C. Matthies, Diploma Thesis, University of Hamburg (1991).

[61] D. Schleicher, Diploma Thesis, University of Hamburg (1991).

[62] N. Wulff, Diploma Thesis, University of Hamburg (1990).

[63] B. Simon, Ann. Phys. **146** (1983) 209.

[64] M. Sieber and F. Steiner, Phys. Lett. **A 148** (1990) 415.

[65] M. V. Berry, Eur. J. Phys. **2** (1981) 91.

[66] B. Eckhardt and D. Wintgen, J. Phys. **B 23** (1990) 355.

[67] M. V. Berry and M. Tabor, Proc. Roy. Soc. London **A 356** (1977) 375.

[68] C. E. Porter, *Statistical Theories of Spectra: Fluctuations*, Academic Press, New York (1965).

[69] M. L. Mehta, *Random Matrices and the Statistical Theory of Energy Levels*, Academic Press, New York (1967).

[70] G. M. Zaslavskii, Sov. Phys. JETP **46** (1977) 1094.

[71] O. Bohigas, M.-J. Giannoni and C. Schmit, Phys. Rev. Lett. **52** (1984) 1.

[72] O. Bohigas, M.-J. Giannoni and C. Schmit, in *Quantum Chaos and Statistical Nuclear Physics*, edited by T. H. Seligman and H. Nishioka, Springer Lecture Notes in Physics No. 263 (1986) 18.

[73] J. H. Hannay and A. M. Ozorio de Almeida, J. Phys. **A 17** (1984) 3429.

[74] T. H. Seligman, J. J. M. Verbaarschot and M. R. Zirnbauer, Phys. Rev. Lett. **53** (1984) 215; J. Phys. **A 18** (1985) 2751.

[75] M. Robnik, J. Phys. **A 17** (1984) 1049.

[76] H.-D. Meyer, E. Haller, H. Köppel and L. S. Cederbaum, J. Phys. **A 17** (1984) L 831.

[77] J. R. Kuttler and V. G. Sigillito, SIAM Review **26** (1984) 163.

[78] E. J. Heller, Lectures given at the Les Houches school on Chaos and Quantum Physics (August 1989), to be published by North-Holland.

[79] H. v. Helmholtz, J. reine u. angew. Math. **57** (1860) 1.

[80] A. Sommerfeld, Jahresber. Dt. Math.-Ver. **21** (1912) 309.

[81] R. E. Kleinman and G. F. Roach, SIAM Review **16** (1974) 214, and references therein.

[82] A. J. Burton and G. F. Miller, Proc. Roy. Soy. London **A 323** (1971) 201.

[83] R. J. Riddell, J. Comput. Phys. **31** (1979) 21 and 42.

[84] M. V. Berry and M. Wilkinson, Proc. Roy. Soy. London **A 392** (1984) 15.

[85] H. P. Baltes and E. R. Hilf, *Spectra of Finite Systems*, B.I.-Wissenschaftsverlag, Mannheim (1976).

[86] B. Simon, J. Funct. Anal. **53** (1983) 84.

[87] F. Steiner and P. Trillenberg, J. Math. Phys. **31** (1990) 1670.

[88] T. A. Brody, J. Flores, J. B. French, P. A. Mello, A. Pandey and S. S. M. Wong, Rev. Mod. Phys. **53** (1981) 385.